ISSN: 2977-0041

Review article

Journal of Material Sciences and Engineering Technology

Common Misconceptions in Piezoelectric Researchers

Kenji Uchino

The Pennsylvania State University, University Park, PA 16802, USA

*Corresponding author
Kenji Uchino, The Pennsylvania State University, University Park, PA 16802, USA.

Received: March 20, 2026; **Accepted:** April 08, 2026; **Published:** April 15, 2026

ABSTRACT

The development of piezoelectric actuators necessitates an interdisciplinary approach, encompassing knowledge from multiple areas, including materials physics and chemistry, electrical and mechanical engineering, and design and marketing strategies. The dissemination of erroneous information is a phenomenon that occurs due to the dearth of knowledge possessed by researchers who are new to the field. This phenomenon can be attributed to the presence of misconceptions, which consequently result in a delay in the innovative developments of the subsequent generation. This paper serves as an instructive tutorial, aiming to rectify common misconceptions among researchers in the fields of ferroelectric and piezoelectric domains. The text reviews the top 12 misconceptions among recent publications, primarily related to the misunderstanding of the following terms relevant to this area: "Voltage and Electric Field," "Ionic Displacement and Strain," "Mistake in Strain Measurement," "Boundary Condition Dependence of Permittivity and Elasticity," "Energy Transmission Coefficient and Efficiency," "Thin Film Device Designing," "Piezoelectric Vibration Damping," "Mechanical Impedance Matching," "Piezoelectric Energy Harvesting," "Resonance and Anti-Resonance," "System Design Principle," and "Best-Selling Devices." These topics were followed by their rectifications, which aimed to promote future smooth progress in piezoelectric actuators.

Keywords: Piezoelectric Actuator, Strain, Efficiency, Energy Transmission Coefficient, Mechanical Impedance Matching, Resonance/Antiresonance, Piezoelectic Energy Harvesting, Pecking Order

INTRODUCTION

The author prepared a manual titled "Ferroelectric Devices and Piezoelectric Actuators" with the objective of providing assistance to instructors teaching their courses [1]. The manual was developed in response to the instructional needs of the instructors who were utilizing the textbooks "Ferroelectric Devices" and "Micromechatronics" [2,3]. However, in response to a considerable number of requests from junior professors, the decision was made to publish several topics as journal papers for a broader audience. These papers, titled "Research Misconceptions and Rectifications, Part I and Part II", were published in 2019 [4,5]. I have received numerous acknowledgements from researchers worldwide. Given their status as professors or senior researchers, it is conceivable that they may have been reluctant to pose fundamental questions to their peers.

The objective of authoring this book chapter, entitled "Common Misconceptions in Piezoelectric Researchers," is to enhance pedagogical competencies. This article is a comprehensive version of the topics, taking into account the still-continuing problematic publications. Despite the fact that the aforementioned misconceptions stem from nearly identical fundamental points in "piezoelecticity," the present article focuses on the misconceptions recently identified in journal articles that have undergone peer review. This finding suggests that both authors and reviewers encounter similar challenges. It is requested that any potential overlap with inquiries previously addressed in the publication be excused. Uchino's objective is not to accuse these authors; rather, he has cited them to address prevalent misconceptions among contemporary researchers in the field of piezoelectricity. Consequently, the author cited a total of 3-10 publications for each "Question" below; however, he demonstrated reluctance to cite these publications in "References."

RESEARCHER'S COMMON MISCONCEPTIONS ON PIEZOELECTRIC ACTUATORS

The utilization of piezoelectric materials as electric components has its origins in the 1950s. Subsequently, during the late 1970s,

Citation: Kenji Uchino. Common Misconceptions in Piezoelectric Researchers. J Mat Sci Eng Technol. 2026. 4(2): 1-24. DOI: doi.org/10.61440/JMSET.2026.v4.110

these elements were incorporated into mechanical components, specifically "piezoelectric actuators," as designated by Uchino. The development of piezoelectric actuators necessitates an interdisciplinary approach, encompassing knowledge in materials physics, electrical and mechanical engineering, and thin film MEMS (micro electro-mechanical system) fabrication processes. Additionally, the design and marketing strategies play a crucial role in the overall development of these actuators. Due to the dearth of knowledge regarding the pedagogical practices of recently-appointed professors, students are occasionally subjected to erroneous instruction, which hinders their ability to engage with innovative developments in the future. This article undertakes a critical review of the most prevalent 12 misconceptions that have been identified in a series of published articles. A significant proportion of these misconceptions pertain to the erroneous interpretation of "Voltage and Electric Field," "Ionic Displacement and Strain," "Mistake in Strain Measurement," "Boundary Condition Dependence of Permittivity and Elasticity," "Energy Transmission Coefficient and Efficiency," "Thin Film Device Designing," "Piezoelectric Vibration Damping," "Mechanical Impedance Matching," "Piezoelectric Energy Harvesting," "Resonance and Anti-Resonance," "System Design Principle," and "Best-Selling Devices."

In the event that the reader is unable to find suitable answers to the following "Questions," it is advisable to read through this tutorial article in its entirety, as it will serve as a prescription for future success. Drawing upon the author's extensive background, which includes 51 years of experience as a university professor, 21 years as a company president or vice president, and 7 years as a government program officer, Uchino has developed a robust philosophy: As the fundamental understanding of the subject matter is critical for the conception of breakthrough inventions, it is imperative to develop a robust foundation of knowledge in this area. It is presupposed that the reader has the fundamental knowledge outlined in References [2,3].

VOLTAGE AND ELECTRIC FIELD

Question 1: As illustrated in Figure 1(a), the polarization is depicted by the solid line, as a function of electric field in the PZT specimen. This is cited from a journal article authored by a distinguished professor of materials. It is imperative to acknowledge the presence of an asymmetric *P-E* hysteresis curve under consideration deviates from the curves typically cited in standard textbooks. Based on the hysteresis curve, the professor posited that "the internal 'positive' electric field bias was observed in the PZT material." Readers are invited to identify the misconception in the claim and elucidate the reason for its occurrence in their experiment.

Solution: It is expected that the reader has acquired the knowledge of the distinction between "voltage" and "electric field" by the time they complete their secondary education. Nevertheless, due to an absence of adequate practical training, a misapprehension analogous to the aforementioned example may have occurred. When the top and bottom surfaces of a PZT plate are electroded, then high DC voltage is applied on the top by keeping the bottom electrode ground (see Figure 1(b)), is this plate poled upward or downward? The accurate response to this inquiry is "downward" with respect to the electric field *E* The direction is determined by recalling the established relationship between electric field and voltage: E=-*grad*(V) If we believe this solid-line $P - E$ hysteresis curve measurement corrects, we need to conclude that the 'negative internal electric field bias' is observed in the hysteresis curve, because this specimen needs just a small negative field to realize the polarization reversal to $-P_S$ while a much larger positive field to realize another reversal to $+P_S$

Nevertheless, the aforementioned professor endeavored to argue the conclusion of "positive field bias." An analysis of the subject's $P - E$ curve reveals an apparent deviation from expected norms. In the course of conducting a practical measurement with a Sawyer-Tower circuit, a research assistant generally determines the voltage-versus-charge relation, and the majority of researchers typically observe positive voltage in the rightward direction. The issue generally manifests during the subsequent step, namely, the conversion of voltage to electric field. In the research community, a common practice is to modify the horizontal scale by dividing the voltage V It is imperative to note that the alteration of the hysteresis curve shape is not a requisite component in this process. Recalling that the field is given by E=-*grad*(V) the electric field is obtained by ($-V/t$) under the supposition that the electric field is distributed uniformly along thickness. In plotting E, the direction is antithetical to the voltage axis. Then, in practice, the hysteresis curve should be rotated 180° with respect to the origin (0,0). As illustrated in Figure 1(a), the dashed curve identifies the presence of a "positive" bias field accurately. It is reasonable to hypothesize that an error occurred during the exchange of the axis direction by the research assistant: $E=V/t$.

Reminder: Do not forget "minus" when you convert the voltage to electric field; $E=-V/t$. The reader needs to instruct your research assistant to exchange the horizontal axis direction, especially in discussing the internal electric field bias direction.

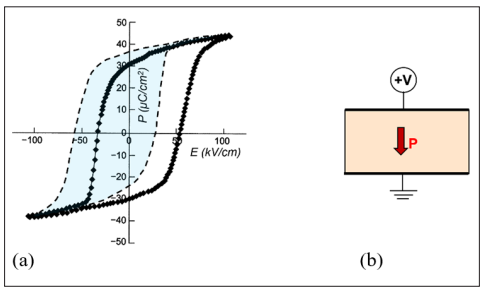

Figure 1: (a) P-E hysteresis curves with internal electric field bias: Original Figure on the paper (solid line), and rectified Figure (dashed line). (b) Visualization of applied voltage and poling direction

IONIC DISPLACEMENT AND STRAIN

Question 2: According to the description provided by a renowned encyclopedia, "Electrostriction is defined as the phenomenon of ions within a crystal lattice displacing slightly under the influence of an external electric field. This displacement will accumulate throughout the bulk, resulting in an overall strain along the field." It is imperative to ascertain whether the preceding statement is accurate or not. Please elucidate the fallacy in this description. A similar mistake is also described in the current multiple textbooks. Intriguingly, the AI software, 'Copilot,' currently offers the "following reference to the author's book [2]."

Solution: The process by which a strain is induced in a crystal through the application of an electric field warrants further investigation. We will examine the simplest ionic crystal, such as NaCl-type, as illustrated in Figure 2 [2]. In a 1-D rigid-ion with spring model of the crystal lattice, springs connecting cations and anions represent the cohesive force resulting from the electrostatic Coulomb energy and the quantum mechanical repulsive energy. As demonstrated in Figure 2(a), the non-centrosymmetric general case is presented. In contrast, Figure 2(b) presents a centrosymmetric scenario. While the spontaneous asymmetry structure does not manifest in this elementary crystal in theory, it is contemplated hypothetically. In scenario 2(a), the springs connecting the ions are subject to variation depending on the ionic distance, with the potential for both hard and soft springs to exist alternately. Conversely, in scenario 2(b), the uniformity of the springs connecting the ions is imperative due to the crystal's inherent symmetry.

In the following section, the state change of the crystal lattice under an electric field applied is considered. As illustrated in Figure 2(a), two "hard" and "soft" springs can be alternatively aligned. When an external electric field is applied to this crystal (as illustrated on the rightward), the cations are drawn in the direction of the electric field, while the anions are drawn in the opposite direction. This results in a relative change in the interionic distance. Depending on the direction of the electric field, the soft spring experiences a greater degree of expansion or contraction compared to the corresponding degree of expansion or contraction of the hard spring. This results in the occurrence of strain x, that is, a unit cell length changes proportionate to the electric field E. This is the 'converse piezoelectric effect.' When expressed as

$$x = dE \tag{1}$$

the proportionality constant d is called the 'piezoelectric constant.'

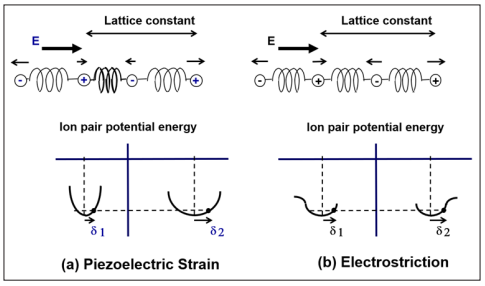

Figure 2: Microscopic explanation of the piezostriction (a) and electrostriction (b). The electrostriction is derived from the inherent nonlinearity of the lattice springs

In contrast, as illustrated in Figure 2(b), the extent of extension and contraction of the spring are nearly equivalent, although ionic displacements bear a resemblance to those observed in Figure 2(a). The separation between the two cations (i.e., the lattice parameter) remains relatively constant, thereby indicating a state of zero strain. The assertion under discussion constitutes the primary rationale for the author's declaration of the aforementioned "Encyclopedia" as a work of misinformation. However, more precisely, ions are not connected by such idealized springs (those are called harmonic springs, in which force (F) = spring constant (k) × displacement (δ) holds). In most cases, the crystal springs possess anharmonicity ($F = k_1\delta - k_2\delta^2$); that is, they are somewhat easy to extend, but hard to contract (because of significantly large quantum mechanical potential during squeezing). Subtle variations in the displacement result in alterations to the lattice parameter, thereby inducing strain that remains unaffected by the direction of the applied electric field (+E or -E). Consequently, this strain is an even function of the electric field, i.e., the square of E). This is called the 'electrostrictive effect,' and can be expressed as

$$x = M E^2 \tag{2}$$

where M is the electrostrictive constant. Note that a small electrostriction crystal does not mean small ionic displacement, but that the anharmonicity of the crystal springs is small.

Reminder: Despite the similarity in ionic displacements (δ) depicted in Figures 2(a) and 2(b), the strain (defined as the differentiation of the displacement $\frac{\partial\delta}{\partial x}$) is distinctly disparate. It is imperative to note that strain does not signify the mere accumulation of ion displacement; rather, it is the result of subtraction or differentiation.

MISTAKE IN STAIN MEASUREMENT

Question 3: Over the course of a decade, Uchino received multiple misconception manuscripts as Editor-in-Chief of various academic journals. Some of these manuscripts reported on a discovery of "giant piezoelectric strains higher than 1%" in PZT ceramic plate samples. Refer to Figure 3(a) as an example, which illustrates the displacement at the disk center and apparent strain (i.e., divided by the sample thickness) as a function of the applied voltage and electric field. The author ascertained that the erroneous assumptions of the aforementioned submitters stemmed from an inaccuracy in their strain measurement, which was typically derived from a direct longitudinal strain measurement (d_{33}) with rectangular-shaped plate samples. The researchers who submitted these manuscripts were distributed from all areas of 'Materials,' 'Electrical,' and 'Mechanical Engineering,' who are not familiar with the weak points of each measuring technique. Now, the reader is hereby invited to engage in a theoretical discourse on the issue of erroneous giant strain measurement. In the event that the reader should discern a considerable discrepancy between the PZT disks, it is imperative to refer to Question 3.

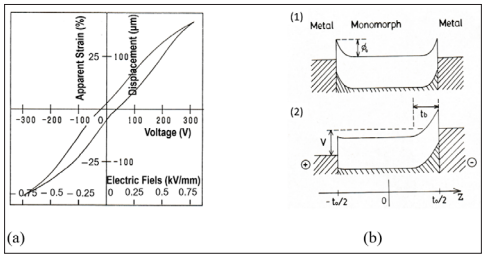

Figure 3: (a) Monomorph characteristics of $0.7Pb(Zr_{0.9}Ti_{0.1})O_3$-$0.3(K_{1/2}Bi_{1/2})ZrO_3$ n-type ceramics. (b) Energy barrier model for an n-type semiconductive monomorph device under zero (1) and V (2) of applied voltage V. The parameters φ_0 and t_0 are a barrier height and a barrier thickness, respectively

Solution: A prevalent method of evaluating piezoelectric actuators involves the utilization of contact (e.g., differential transformer, eddy-current type) and non-contact (e.g., laser vibrometer) displacement sensors on the piezoelectric plate surface, which is positioned on a flat table. These sensors are utilized in conjunction with an alternating current (AC) voltage applied to the specimen. In instances where the sample geometry is cubical—that is to say, where the thickness is commensurate with the surface area — the strain of the sample can be reasonably evaluated by the ratio of the measured displacement divided by the sample thickness. However, in the case of a plate-like sample geometry (i.e., thickness << length, width), erroneous data can occasionally be derived due to the potential for deformation resulting from the bending of the plate. The surface center of the bending plate-like specimen demonstrates a displacement that is considerably greater than the pure strain deformation. Given the standard strain level of 0.1% for PZT ceramics, when the apparent strain—that is, the displacement divided by the sample thickness—exceeds 1%, it is imperative to consider the potential for bending deformation before concluding that a substantial strain has been reached.

Monomorph

An innovation, dubbed "Monomorph" by Uchino et al. offers a compelling proposition to the reader [6-9]. The reader may already be acquainted with the concepts of "bimorphs" and "unimorphs," which are frequently utilized in speaker and microphone applications. A conventional bimorph bending actuator consists of two piezoelectric plates or a combination of two piezoelectrics and an elastic shim that are bonded together. However, the bonding layer has been observed to induce two notable effects: an increase in hysteresis and a degradation of the displacement characteristics. The delamination problems have been documented. In addition, the fabrication process for such devices is laborious and costly. It involves several steps, including cutting, polishing, electroding, and bonding. Consequently, a monolithic bending actuator (monomorph) that does not necessitate bonding represents a highly compelling alternative structural design.

The operating principle is predicated on the combined action of a semiconductor contact phenomenon and the piezoelectric effect. The application of metal electrodes to both surfaces of an n-type semiconductor plate, in conjunction with the application of a voltage, as illustrated in Figure 3(b), results in the concentration of the electric field on one side. This process gives rise to the formation of a "Schottky barrier," thereby generating a non-uniform field within the plate [6]. When the piezoelectric is slightly semiconducting, contraction along the surface occurs through the piezoelectric d_{31} effect only on the side where the electric field is concentrated. The non-uniform field distribution generated in the ceramic causes an overall bending of the entire plate. Referring which provides the physical formula on the barrier thickness t_0 with barrier height and applied voltage V, since the barrier thickness φ_0 should be in comparable with the plate thickness, we can calculate the desired donor density [6]. Research was conducted on $Pb(Zr,Ti)O_3$-based piezoelectric ceramics with the semiconducting properties required for use in these monomorph devices [9]. Modified PZT with the exact composition $0.7Pb(Zr_{0.9}Ti_{0.1})O_3$-$0.3(K_{1/2}Bi_{1/2})ZrO_3$ were prepared from a solid solution with the n-type semiconductor perovskite compound $(K_{1/2}Bi_{1/2})ZrO_3$ to obtain suitable electrical properties. A ceramic plate (20 mm long, 10 mm wide, and 0.4 mm thick) with surface electrodes was fixed in a cantilever style. Under the application of 300 V, a maximum tip deflection close to 200 μm could be obtained (Figure 3(a)). The apparent strain was hereby calculated by dividing the given value by the thickness of the PZT plate. This deflection is analogous to the optimal deflection level of a bimorph device. It is imperative to acknowledge that the height of the barrier is a critical factor that must be taken into consideration. The response is contingent upon the type of metal electrode utilized: Figure 3(a) is when the Ag electrode was utilized, while the ohmic InGa electrode did not demonstrate significant deflection [6]. It is also noteworthy to observe the correlation between electric conductivity and crystal structure within the $Pb(Zrx,Ti1\text{-}x)O_3$ system. As the reader may recognize, there is a morphotropic phase boundary (MPB) around the composition (52,48) between rhombohedral and tetragonal phases. Despite the attainment of reasonable semiconductivity in both the Rhomb and Tetra phases, the MPB compositions were unable to manifest monomorph characteristics due to their elevated resistivity.

Soft and Hard PZT

The reader is probably acquainted with the fact that PZT piezoelectric performance is easily modified by changing small amount of dopants. The terminologies "Hard" and "Soft" on the near-MPB $Pb(Zr^{4+},Ti^{4+})O^{2-}_3$ piezo-ceramics are introduced by clarifying the mechanism difference. Donor doping (such as Nb^{5+} in the B^{4+} site) tends to facilitate domain wall motion, leading to enhanced piezoelectric charge coefficients, d, and electromechanical coupling factors, k, producing what is referred to as a 'soft piezoelectric'. Conversely, acceptor doping (such as Fe^{3+} in the B^{4+} site) tends to pin domain walls and impeding their motion, leading to an enhanced mechanical quality factor, Q_m, producing what is called a 'hard piezoelectric' [10].

Soft piezoelectric materials are distinguished by their comparatively high permittivity $\varepsilon_0\varepsilon^X$ and high piezoelectric charge coefficients d. It has been demonstrated that these devices are applicable in situations that necessitate a rapid response time. Examples of such devices include inkjet printers and fuel injection valves. Nevertheless, soft piezoelectrics generate a considerable amount of heat when driven at resonance. This phenomenon is attributed to their relatively low mechanical quality factor Q_M. Therefore, for high-power applications, such as ultrasonic motors and transformers, hard piezoelectrics with a larger mechanical quality factor and vibration velocity are preferred, despite the slight sacrifices incurred with respect to their smaller piezoelectric strain coefficients d.

The acceptor-doping is important to render PZT ceramics "hard" (large coercive field) through the establishment of domain-wall pinning with oxygen vacancy. This section is finally devoted to the presentation of a novel microscopic model that elucidates the genesis of the "internal bias field" growth in very hard PZT ceramics. This phenomenon was previously demonstrated in Figure 1. The presence of oxygen deficiencies and the relatively slow growth rate of the mechanical quality factor Q_M, which was measured at a couple of hours, are the basis for this conclusion. The "oxygen deficiency diffusion" model is illustrated in Figure 4 [11]. In the context of the electric poling process, the defect

dipole P defect—defined as a pair of acceptor ions and oxygen deficiency—will be arranged in a parallel configuration with respect to the external electric field (see Figure 4, Left). Subsequent to the removal of the field, the process of oxygen diffusion ensues. This diffusion can be estimated on a scale of hours at ambient temperature (see Figure 4, Right). In consideration of the slight variations in atomic distances between the A and B ions within the perovskite crystal in a ferroelectric (asymmetric) phase, the oxygen diffusion probability is predicted to exhibit a modest increase for the downward direction, as illustrated schematically in the accompanying figure. This phenomenon is expected to result in an augmentation in the defect dipole with the passage of time. This phenomenon may be the origin of the "internal positive bias electric field" growth, as shown in Figure 1. It is evident that the dipole alignment is unidirectionally fixed along the polarization direction.

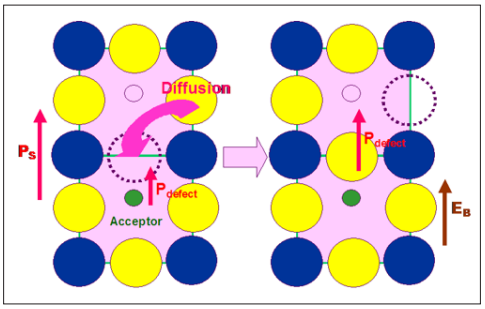

Figure 4: Oxygen deficiency diffusion model for explaining the internal bias electric field growth [11]. The oxygen diffusion may take 1 – 2 hours at room temperature after electric poling

Reminder: Donor doped PZT-based ceramic plates demonstrate "bending deformation" in response to electric field application, yielding erroneous strain levels that vary depending on the measuring technique. This "monomorph" deformation has been observed in both rhombohedral and tetragonal phases, though it diminishes interestingly around the morphotropic phase boundary (MPB) compositions.

BOUNDARY CONDITION DEPENDENCE OF PERMITTIVITY AND ELASTICITY

Question 4: In a couple of papers published in a Mechanical Engineering-related journal, we found a sentence that stated, "Since elastic compliance and sound velocity are the constants in a piezoelectric material, the resonance frequencies are solely determined by the sample size." What are the shortcomings of this author's statement? You may use $f_R = v/2L = 1/(2L\sqrt{\rho s_{11}^E})$..

Definition of Electromechanical Coupling Factor

Firstly, the reader is prompted to recall the following constitutive equations [2,3]:

$$D = \varepsilon_0 \varepsilon^X E + dX \quad (3)$$

$$x = dE + s^E X \quad (4)$$

where d is the piezoelectric constant, $\varepsilon_0\varepsilon^X$ and s^E are the permittivity under stress-free condition, and elastic compliance under short-circuit condition, respectively. Then, the 'electromechanical coupling factor k' is defined by

$$k^2 = d^2/\varepsilon_0 \varepsilon^X s^E. \quad (5)$$

Alternatively, the electromechanical coupling factor k^2 is defined as the "energy conversion rate" between electric and mechanical energy.

k^2 = (Stored mechanical energy)/(Input electrical energy). (6a)

or

k^2 = (Stored electrical energy)/(Input mechanical energy). (6b)

Constraint Dependence of Permittivity and Elastic Compliance in Piezoelectrics

Solution: In a piezoelectric coupling material, it is important to learn the boundary conditions under which a material is operated when characterizing the dielectric constant and elastic compliance of a piezoelectric material [3]. The application of a constant electric field E_0 is a critical component of the experimental setup. As illustrated in Figure 5(a), when the input electrical energy is applied to a piezoelectric sample, it will vary depending on the mechanical conditions to which the material is subjected. These mechanical conditions can be categorized into two distinct states: (1) The "mechanically clamped state," designated as "constant strain," involves the maintenance of a constant strain level that precludes specimen deformation. This condition is characterized merely by the electrostatic energy. (2) The "mechanically free state," is characterized by the absence of external forces that would merely provide mechanical energy on the specimen. It is free to deform under electrically short-circuit condition. It is hypothesized that the total input electrical energy under the free condition will be the sum of the energy associated with pure electrostatic energy (without deformation) and the pure mechanical energy under a short-circuit condition. Taking into account $x = dE_0$, this can be expressed by:

$$\frac{1}{2}\varepsilon^X \varepsilon_0 E_0^2 = \frac{1}{2}\varepsilon^x \varepsilon_0 E_0^2 + \frac{1}{2s^E}x^2 = \frac{1}{2}\varepsilon^x \varepsilon_0 E_0^2 + \frac{1}{2}\frac{d^2}{s^E}E_0^2 \quad (7a)$$

So that using the electromechanical coupling factor k in Eq. (5):

$$\varepsilon^X \varepsilon_0 = \varepsilon^x \varepsilon_0 + \frac{d^2}{s^E} \text{ or } \varepsilon^x = \varepsilon^X (1-k^2) \quad (7b)$$

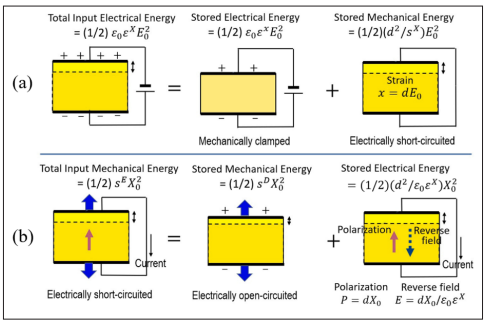

Figure 5: Schematic representation of the response of a piezoelectric material under: (a) constant applied electric field and (b) constant applied stress conditions

Next Figure 5(b) demonstrates that constant stress X_0 has a detrimental effect on the piezoelectric body. The application of the piezoelectric effect results in a distinct variation in the input mechanical energy, contingent upon two specific electrical conditions. (1) The "open-circuit state." It is imperative to note that a constant electric displacement is maintained (or

high voltage is generated) in this context, as expressed by $\varepsilon^X \varepsilon_0 E=dX_0$. (2) The "short-circuit state." The piezoelectric material is subjected to zero electric field by generating a current originated from $D=dX_0$. It is hypothesized that, in the context of a short-circuit condition, the total mechanical energy input should be the sum of the mechanical energy under open-circuit conditions and the electrical energy converted via the direct piezoelectric effect. This can be expressed as:

$$\frac{1}{2}s^E X_0^2=\frac{1}{2}s^D X_0^2+\frac{1}{2}\varepsilon^X \varepsilon_0 E^2=\frac{1}{2}s^D X_0^2+\frac{1}{2}\frac{d^2}{\varepsilon^X \varepsilon_0}X_0^2 \quad (8a)$$

which leads to:

$$s^E=s^D+\frac{d^2}{\varepsilon^X \varepsilon_0} or\ s^D=s^E(1-k^2) \quad (8b)$$

The reader is capable of comprehending the concept of smaller permittivity ε^x under clamped conditions, because of an additional elastic energy. In the case of smaller s^D (or stiffer elasticity) under open-circuit, a high reverse electric field is generated by the application of stress, thereby suppressing the strain generated in the piezoelectric. This scenario is re-examined in **Section 2.10** Resonance and Antiresonance Modes. Consequently, both permittivity and elastic compliance can be tuned in a piezoelectric material by changing the external conditions.

Reminder: The permittivity and elastic compliance of a piezoelectric change significantly according the external constraints. The ratio of the permittivity under strain-free and stress-free conditions, as well as the ratio of the elastic compliance under open-circuit and short-circuit conditions are both given by $(1 – k^2)$, where k is the electromechanical coupling factor.

Dielectric constant: $\varepsilon^x/\varepsilon^X=(1-k^2)$ (9)
Elastic compliance: $s^D/s^E=(1-k^2)$ (10)

ENERGY TRANSMISSION COEFFICIENT AND EFFICIENCY

Question 5: A mechanical engineering professor described in his paper: "A 'coupling coefficient' is a measure of the 'efficiency' with which a piezoelectric material converts the energy in an imposed signal to useful mechanical energy," and "By applying 1 J of electric energy to a piezoelectric with an electromechanical coupling factor k, we accumulate k^2 J of mechanical energy in this piezo-material. Thus, this actuator can work mechanically up to k^2 J to the outside, and the efficiency is considered to be k^2 %." These sentences include two major misconceptions. The reader is requested to describe them and provide their rectifications.

Solution: This is a common misconception among mechanical engineering researchers, who may not be aware of the methods for recovering electrostatic energy from a piezoelectric. This subsection presents three analogous terminologies that may provide the necessary rectifications to **Question 5.**

Electromechanical Coupling Factor

As is described in **Section 2.4.1**, the electromechanical coupling factor is given by three parameters: d = piezoelectric constant, s^E = elastic compliance under short-circuit condition, and ε^X = permittivity under stress-free condition, as in Eq. (5) $k^2=d^2/\varepsilon^X s^E$. The value k^2 has a meaning of 'energy conversion rate,' that is,

$$\begin{cases} k^2=(\text{Stored mechanical energy})/(\text{Input electrical energy}) \\ k^2=(\text{Stored electrical energy})/(\text{Input mechanical energy}) \end{cases}$$

For the sake of illustration, let us consider a piezoelectric pseudo-DC device with a value of k= 50% for example. If we then consider a value of k^2 = 25%, it can be demonstrated that the input electrical energy 100 is converted into mechanical energy 25 by the remaining quantity as the stored electrical energy $(1-k^2)\approx 74$. This energy is stored in a capacitor. It has been established that, given the loss factor (dielectric loss tan δ) is less than 1%, the actual dissipated loss as heat is generally less than 1% as well. As illustrated in Figure 6(a), the energy conversion process is represented schematically. Consequently, if the stored electrical energy can be successfully recovered and reintroduced into the driving circuit, the loss can be constrained to a mere 1%.

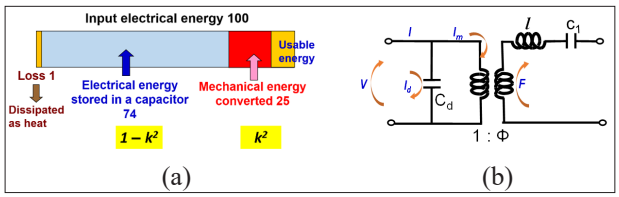

Figure 6: (a) Energy conversion rate in a typical piezoelectric. (b) Equivalent circuit (k_{31} mode)

Energy Transmission Coefficient

It has been demonstrated that not all of the mechanically stored energy can be utilized. The execution of the work is contingent upon the mechanical load (Figure 7(a)). In the absence of mechanical load or complete clamp condition (i.e., no strain), no output work is performed, and no energy is expended externally. Therefore, the maximum "energy transmission coefficient" is defined as follows:

$$\begin{cases} \lambda_{max}=(\text{Output mechanical energy})/(\text{Input electrical energy})_{max} \\ \lambda_{max}=(\text{Output electrical energy})/(\text{Input mechanical energy})_{max} \end{cases}$$

The difference of the above from Eqs. (6) and (11) is "stored" or "output/spent" in the numerator.

We shall initiate our examination with the most elementary scenario, in which an electric field, designated as E, is abruptly applied to a piezoelectric specimen under constant external stress (i.e., load), X, defined as the compressive stress. This phenomenon can be understood by examining the application of force and voltage to the actuator. As illustrated in Figure 7(a) [3], the force and voltage are applied to the actuator in a "step" function, rather than a gradual application. As illustrated in Figure 7(b), two electric-field versus induced-strain curves are presented, corresponding to two distinct conditions: one under the presence of a mass load and another in the absence of a mass load. Given that the area on the field-strain domain is not indicative of the energy, it is necessary to utilize the stress-strain and field-polarization domains independently for the purpose of discussing mechanical and electrical energy, respectively. As demonstrated in Figure 7(c), the calculation of mechanical

energy is illustrated. It is imperative to acknowledge that the mass initiates the reduction in size of the actuator, initially by s^X (s signifying the compliance of the piezo-material, with X being less than zero). The mechanical energy sX^2 can be conceptualized as a form of "loan" from the actuator to the mass. This energy is subsequently returned or deducted at a later point. The energy under consideration is congruent with the hatched area depicted in Figure 7(c). The application of a step electric field results in the expansion of the actuator to the strain level dE under constant stress conditions. The quantity of mechanical energy supplied by the actuator (i.e., electromechanically transduced energy) to the mass is equivalent to the magnitude of the following expression: |dEX|. As with the repayment of the initial "loan," the output work (from the actuator to the mass) can be calculated as the area subtraction (illustrated by the dotted area in Figure 7(c)).

$$\int(-X)\,dx = -(d\,E + s\,X)\,X. \tag{12}$$

Conversely, Figure. 7(d) illustrates the electrical energy calculation process. The mass load X generates the "loan" electrical energy by inducing P=dX (see the hatched area in Figure. 7(d)). By applying a 'step' function electric field E, the actuator (like a capacitor) receives the electrical energy of $\varepsilon_0\varepsilon E^2$. Thus, the total energy is given by the area subtraction (shown by the dotted area in Figure. 7(d))

$$\int(E)\,dP = (\varepsilon_0\varepsilon\,E + d\,X)\,E. \tag{13}$$

Now, we need to choose a proper load to maximize the 'energy transmission coefficient' λ defined by the ratio between Eqs. (12) and (13). It is imperative to consider the maximization condition of

$$\lambda = -(d\,E + s\,X)X/(\varepsilon_0\varepsilon\,E + d\,X)E,$$

to achieve the maximum energy transmission coefficient in Eq. (11). The detailed calculation process can be found in Section 3.2 of Ref. [3].

$$\lambda_{\max} = \left[(1/k) - \sqrt{(1/k^2) - 1}\right]^2 = \left[(1/k) + \sqrt{((1/k^2) - 1)}\right]^{-2} \tag{14}$$

When the application of stress or electric field is considered to be gradual, the energy terms necessitate the value of (1/2) to ensure consistency as $\frac{1}{2}s^E X^2$ or $\frac{1}{2}\varepsilon_0\varepsilon^E E^2$ respectively. Nevertheless, given the divergent definitions of k^2, λ_{max} and efficiency η, the ratios of the two types of energy are equivalent to the ratios that result from a sudden input application. We can obtain from Eq. (14) for a reasonable k (< 95%) that

$$k^2/4 < \lambda_{max} < k^2/2.$$

For a small k, $\lambda_{max} = k^2/4$ and for a large k, $\lambda_{max} = k^2/2$ It is also worth noting that the maximum condition stated above does not agree precisely with the condition which provides the maximum output mechanical energy. The maximum output energy (by neglecting the input electric energy change) can be obtained when the dotted area in Figure. 7(c) becomes maximum under the constraint of the rectangular corner point tracing on the line (from dE on the vertical axis to –dE/s on the horizontal axis). Therefore, the load should be a half of the maximum generative stress and the mechanical energy: $-[dE - s(dE/2s)](-dE/2s) = (dE)^2/4s$. In this case, since the input electrical energy is given by $[\varepsilon_0\varepsilon\,E + d\,(-dE/2s)]\,E$,

$$\lambda = 1 / 2[(2/k^2) - 1], \tag{15}$$

which is close to the value λ_{max} when *k* is small, but has a different value when k is large, that is predicted theoretically.

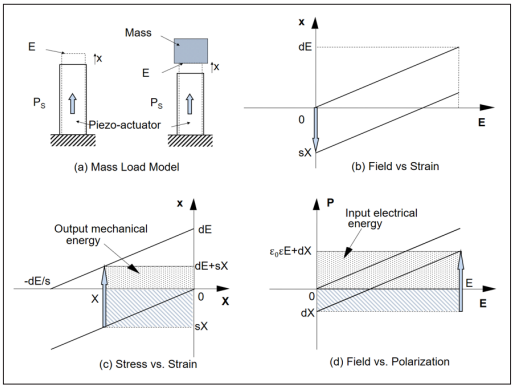

Figure 7: Calculation of the input electrical and output mechanical energy: (a) load mass model for the calculation, (b) electric field versus induced strain curve, (c) stress versus strain curve, and (d) electric field versus polarization curve

Efficiency

Conversely, the "efficiency" parameter is defined by the following equation:

$$\begin{cases} \eta = (\text{Output mechanical energy})/(\text{Consumed electrical energy}) \\ \eta = (\text{Output electrical energy})/(\text{Consumed mechanical energy}) \end{cases}$$

The recovery of the mechanically unconsumed energy, stored in the piezoelectric elastic material (i.e., the "piezo-spring"), would indicate that the consumed electric energy is equivalent to the sum of the output mechanical energy (work done on the exterior) and heat loss. This approach yields a remarkable result, with a 99% efficiency rate, signifying a high level of effectiveness.

In the absence of knowledge among mechanical engineers regarding the recovery of electrostatic energy stored in the actuator/capacitor, the decision was made to release it by shorting the drive circuit. This action was taken in order to proceed with the subsequent operation. In the context of the present study, it is evident that the efficiency of the system is less than 25% (equivalent to k^2) in the event of the unfavorable scenario.

Drive Circuit for High Efficiency

The recovery of electrostatic energy from a piezoelectric capacitor ($1 - k^2$) in damped capacitance is a subject of interest. Illustrative examples can be found in the applications of dot-matrix/ink-jet printers [18] and diesel injection valve control [19], where multilayer actuators are driven at frequencies less than 1 kHz, which is considerably lower than the resonance frequency. Though the k_{33} mode is different, refer to a simpler equivalent circuit for the k_{31} mode shown in Figure 6(b) (no-loss case is illustrated). In this equivalent circuit, motional current and damped current ($C_d = (1–k^2)C_0$) should have $k^2 : (1–k^2)$ ratio under an off-resonance condition. If we insert the inductance L in the driving system so as to create a resonance circuit of L and C_d under the condition of $\omega^2 = 1/LC_d$ (ω: operation cycle such

as 1 kHz), the electric energy stor capacitance ed in the damped capacitance C_d starts flip-flopping with L, without losing this energy (if we neglect the loss or heat generation). Upon returning to the initial zero-position of the actuation, the electric energy stored in the damped capacitance is transferred to the inductor L. This facilitates the subsequent actuation, which subsequently commences in synchrony with the return of the electric energy to the capacitor C_d. A "negative capacitance" usage constitutes an alternative solution, as the heavy and bulky magnetoelectric inductor poses significant challenges to miniaturization efforts.

Reminder: (1) The "electromechanical coupling factor" is defined as the energy conversion rate. (2) The "energy transmission coefficient" is the proportion of stored mechanical energy (k^2) that is converted into usable mechanical energy by a piezoelectric device. This proportion ranges from 1/4 to 1/2 of the stored energy (k^2). (3) The "efficiency" of the piezoelectric devices is typically high, reaching 99%, provided that the stored electric energy is recovered in a piezo-capacitor with an appropriately selected inductance or a negative capacitance. It is important to note, however, that the conventional coil inductor cannot reduce the size and weight (and Joule loss) of the power supply.

THIN FILM DEVICE DESIGNING

Question 6(a): The research conducted on piezoelectric MEMS (micro electro-mechanical system) has centered on the PZT (lead zirconate titanate) thin film, thickness of which is approximately 1 μm, for actuators and piezo-energy harvesting applications. What are the major issues that must be resolved in a design that has been widely accepted and is depicted in Figure 8, as referenced from a prominent journal?

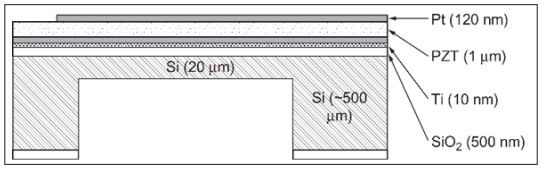

Figure 8: The piezoelectric MEMS structure under consideration has a PZT thin film thickness of approximately 1 μm, which is employed for use as an actuator

Solution: The present design is found to have two major flaws: the generative mechanical power level and the PZT and substrate thickness ratio.

Generative Mechanical Power Level

The acceleration of the commercialization of piezoelectric actuators and transducers for portable equipment applications has led to the identification of a significant bottleneck in piezoelectric devices: substantial heat generation imposes limitations on the maximum power density that can be achieved. Despite the fact that the problem is considerably smaller than that posed by electromagnetic (EM) motors and transformers (i.e., Joule heat from thin conducting wires), the piezoelectric devices become "ceramic heaters" with increasing input/output power. This increase is significant. The utilization of a piezoelectric device at its resonance point results in the initiation of thermal energy production, which is directly proportional to the magnitude of vibration. The vibration velocity that results in a 20°C temperature rise from room temperature is referred to as the "maximum vibration velocity" within this field. This term is employed to ensure safety standards are met, as evidenced by the potential for burns from 50°C electronic components. The maximum handling power of a well-known hard Pb(Zr,Ti)O_3 (PZT) that has been demonstrated thus far is approximately 10 W/cm³ [10]. Taking into account the practically required minimum power levels, 30 – 100 mW for charging electricity into a battery (DC-DC converter spends 2 – 3 mW), 10 – 20 mW for soaking blood from a human vessel, or 1 – 3 mW for sending electronic signal, minimum 1 mW handling is necessary, leading to the minimum PZT volume of 0.1 mm³ [10]. In the context of "nearly-zero" load applications, such as optical beam reflectors and mirrors, the requirement for power is negligible, unless the application necessitates agility. Consequently, MEMS devices with PZT films thinner than 1 μm (the current commercial standard) are not viable for actuator applications. Levels ranging from 1 to 10 μW, typically obtained from 1 μm films, are generally employed as sensors rather than actuators. The utilization of films with a thickness ranging from 10 to 30 μm is recommended, with a device area of 3 × 3 mm², provided that the current materials are utilized and the maximum power density is not exceeded ~10 W/cm³. It is important to note that due to the thermal conduction from the silicon substrate, the PZT can be driven under somewhat higher input electrical energy, leading to a higher maximum vibration velocity. Consequently, the aforementioned estimation may be slightly pessimistic.

PZT/Substrate Thickness Ratio

The fabrication of a unimorph bending actuator entails the bonding of a piezoceramic plate to a metallic shim, as illustrated in Figure 8. The tip deflection, δ, of the unimorph supported in a cantilever configuration (i.e., one end support) is given by:

$$\delta = \frac{d_{31} l^2 Y_c t_c}{Y_m[t_0^2 - (t_0 - t_m)^2] + Y_c[(t_0 + t_c)^2 - t_0^2]} E \tag{17}$$

In this equation, E signifies the electric field applied to the piezoelectric ceramic, d_{31}, the piezoelectric strain coefficient, l, the length of the unimorph, Y, Young's modulus for the ceramic or the metal, and t is the thickness of each material. The subscripts 'c' and 'm' denote the 'ceramic' and the 'metal,' respectively. The quantity t_0 is defined as the distance between the "strain-free neutral plane" and the bonding surface. This distance is calculated according to the following definition:

$$t_0 = \frac{t_c t_m^2 (3t_c + 4t_m) Y_m + t_c^4 Y_c}{6 t_c t_m (t_c + t_m) Y_m} \tag{18}$$

In the case of a unimorph supported at both ends, as illustrated in Figure 8, the center displacement is equivalent to one-quarter of the aforementioned displacement δ, as illustrated in Eq. (17). Consequently, the analytical approach is equivalent [2,3].

From the standpoint of simplicity, under the assumption that $Y_c = Y_m$, the optimal (t_m/t_c) ratio that will maximize the deflection, δ, is calculated. Substituting the t_0 expressed in Eq. (18) into Eq. (17) results in the following equation:

$$\delta = \frac{d_{31} l^2 3 t_m t_c}{(t_m + t_c)^3} E \tag{19}$$

We discuss the optimum (t_m/t_c) ratio under the following two conditions.

A fixed ceramic thickness, t_c

In the event that a PZT plate is to be procured, the purchaser must ascertain the standard thickness of the PZT plate from the company catalog. It is imperative to maximize the function $f = \frac{t_m t_c}{(t_m + t_c)^3}$ while maintaining a constant ceramic thickness, t_c.

$$\frac{\partial f(t_m)}{\partial t_m} = \frac{(t_c - 2t_m)t_c}{(t_m + t_c)^4} = 0 \quad (20a)$$

The metal plate thickness should be $t_m = t_c/2$ and to= $t_c/2$.

A fixed total thickness, $t_c + t_m$

This condition is imperative when there is a necessity to maintain the resonance frequency at a consistent level in order to ensure the desired tone level is preserved. To illustrate this point, consider the role of a sounder/speaker manufacturer. Eq. (19) becomes the following, where $t_{tot} = t_m + t_c$.

$$\frac{\partial f(t_m)}{\partial t_m} = \frac{(t_{tot} - 2t_m)}{t_{tot}^3} = 0 \quad (20b)$$

Thus, it is determined that both the metal and ceramic plate thickness should be $t_m = t_c = t_{tot}/2$ and to= $t_{tot}/3$.

Achieving a substantial displacement necessitates that the thickness of the silicon substrate be comparable to that of the PZT thickness. Muralt's research endeavors centered on the calculation of the electromechanical coupling factor k. The resonance frequency for PZT thin films on a silicon substrate is contingent upon the substrate thickness, with the parameters fluctuating accordingly [12]. The ultrasonic stator utilized in the present studies exhibited a circular geometry, characterized by a radius of 5.2 mm, mode B_{01}, and an $e_{31,f}$ of -6 C/m^2. It is imperative to note that film stresses were excluded from the scope of consideration. As illustrated in Figure 9, the electromechanical coupling demonstrates a maximum value when the silicon thickness is equivalent to the PZT thickness [12].

Reminder: (a) From the generative mechanical power viewpoint (minimum 1 mW for actual applications), the PZT thickness should be higher than 30 μm with area 3×3 mm^2, taking into account the material's maximum vibration velocity. (b) Silicon substrate thickness should be chosen in a similar range of the PZT thickness. The PZT 1 μm on 20 μm silicon membrane design, as illustrated in Figure 8, is intended exclusively for use in sensor applications. It should be noted that this design is not applicable to actuator designs.

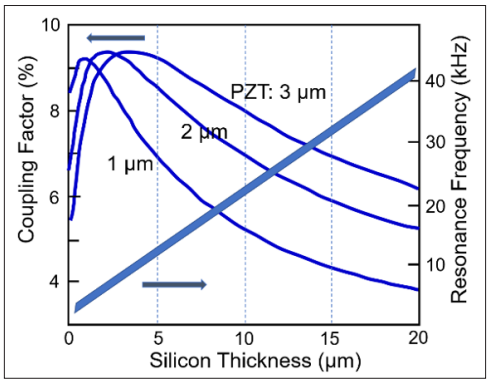

Figure 9: Silicon thickness dependence of the electromechanical coupling factor, k, and the bending resonance frequency of an PZT film ultrasonic circular stator [12]

Question 6(b): The following statements have been observed in the MEMS (micro electro-mechanical system) literature: In the fabrication of PZT thin films, "it is imperative to select a substrate with a lattice parameter that closely matches that of the PZT." This is to ensure that the interface does not undergo a lattice parameter mismatch, which can lead to a degradation in the piezoelectric film's performance. The rationale behind this approach is frequently cited as being due to the findings of preceding researchers. The efficacy of this strategy merits further scrutiny. The reader is invited to determine whether the performance can be enhanced by taking the "large" lattice parameter mismatch.

Solution: In general, the thin film structure is inevitably affected by the following four important factors:

1. **Size constraints:** As a parallel can be drawn with a powder sample in which critical minimum diameters exist around sub μm (e.g., 0.1 μm for Barium Titanate), a critical film thickness may exist below which the ferroelectricity would be significantly degraded or even disappear. However, it should be noted that thin films are energy-stabilized with a large 2D area. The general ferroelectric/piezoelectric degradations were reported for 10–1 μm thickness range in Ref. [13], then, the measurement further falls within the range of 1–0.1 μm range in [14]. For films less than 10 nm in [15], ferroelectricity has still been observed in PZT thin films as low as 2–3 unit cells.
2. **Stress from the substrate:** The discrepancy between the lattice parameters of the substrate and the epitaxial PZT leads to the generation of dislocations within the PZT thin film. This phenomenon results in a deterioration of the film's performance. Additionally, tensile or compressive stress is induced due to thermal expansion mismatch between the film and the substrate. This stress can occasionally result in an elevated coercive field during domain reorientation.
3. **Epitaxial growth:** In addition, the crystal orientation dependence should be taken into consideration, as was the case in single crystals. An exemplar is found in a rhombohedral composition of PZT, which is predicted to demonstrate optimal performance when the P_S direction is oriented at a 57° cant from the film normal direction or the electric field direction (i.e., the (001) perovskite crystallographic orientation). For a more thorough examination of this topic, please refer to the previous paper [16].

4. **Preparation Constraint:** The Si substrate requires a low sintering temperature for the PZT film. In the standard preparation of PZT, the maximum temperature of 800°C for a brief period is generally accepted as the threshold that may impede the crystallization process of the PZT film. This has the potential to diminish the piezoelectric properties of the material.

Wasa's PZT film preparation, characterized by a substantial crystal mismatch devoid of dislocation, is a subject of considerable intrigue. He investigated piezoelectric performance enhancement by using the crystal lattice mismatch intentionally of PZT-based thin films on Si and Sapphire [17]. Referring to Fig. 10(a), the lattice mismatch statuses between the thin PZT film and substrate are considered in the case that the lattice parameter of the piezoelectric film is larger than that of the substrate. When we deposit the film on the substrate, the PZT film will impose compressive stress in the plane direction. However, if the 'misfit rate' is large, dislocations may be generated in every certain-unit lattices. Given the fact that dislocation has been demonstrated to degrade piezoelectric performance to a significant degree, the majority of researchers have historically endeavored to reduce the mismatch rate between the film and substrate. As illustrated in Fig. 10(b), Wasa's preparation method for the strained thin film on the substrate without dislocation involves the visualization of the fine PZT power depositing process on the substrate with a 1.7° angled surface. Because the PZT interface plane changes one-step height every 30 horizontal unit-cells. The lattice misfit stress can be relaxed without generating significant dislocations. This angle can be different, depending on the lattice misfit rate. The PZT films were demonstrated to withstand high compressive stress without dislocation, exhibiting a Curie temperature as high as 600°C, which is 250°C higher than its original Curie temperature under zero stress. It is acknowledged that the Curie temperature can be modified by a rate of 50°C per 1 GPa under hydrostatic pressure [18]. This phenomenon can be exploited to enhance the performance of the film.

Reminder: In the fabrication of PZT films, it is advisable to intentionally manipulate the tensile or compressive stress, while ensuring that the substrate is not subjected to dislocation formation through the application of a slight cant angle of the substrate [17]. This angle can be different, depending on the lattice misfit rate.

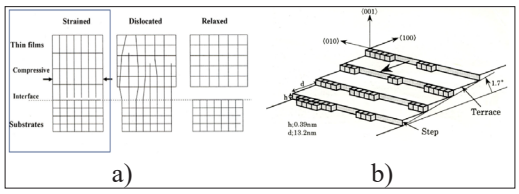

Figure 10: (a) The presence of mismatches in the lattice configurations between the thin film and substrate. (b) The preparation method for the strained thin film on the substrate without dislocation [17]

PIEZOELECTRIC VIBRATION DAMPING

Question 7: The rapid response of the piezoelectric actuator can result in the occurrence of vibration ringing, which occasionally follows the initial response in applications involving the positioner and pulse drive. This problem has been observed during the development of dot printers [19] and diesel injection valves [20]. Since the conventional diesel engine requires much finer fuel mist for burning perfectly, new diesel injection valves were developed with piezoelectric multilayered (ML) actuators with much quicker nozzle needle response. Figure. 11(a) shows such a common-rail type diesel injection valve with a ML piezo-actuator, which produces high pressure fuel and quick injection control (5-time open/close valve operations per one engine cycle of 10 msec) (Figures. 11(b) and 11(c)) [20]. However, the ringing of the valve rod did not stop easily because of the 10 μs level response of the ML, so that these additional fuel injections were a serious problem. Initial attempts by automotive engineers to install mechanical dampers, such as plate springs, to mitigate the vibration ringing proved unsuccessful, as these dampers also significantly reduced the displacement amplitude. Furnish a piezo-drive concept that will effectively mitigate the vibration ringing without compromising efficiency.

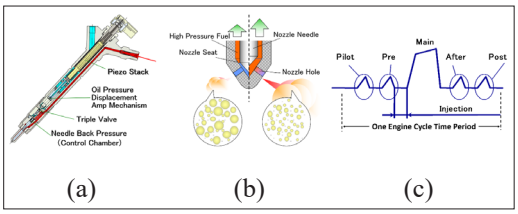

Figure 11: (a) Common rail type diesel injection valve with a piezoelectric multilayer actuator [Courtesy by Denso Corporation]. (b) Illustration on how to create fine fuel mist. (c) multiple injection timing chart

Solution: The 'Pulse Drive' technique proposed by the author's group was highly acknowledged to solve the ringing problem by keeping the same (even larger) displacement of the MLs [21,22].

Longitudinal Vibration through (d_{31}) in a Rectangular Plate

The following investigation will consider the simplest model of longitudinal k_{31} mechanical vibration in a piezoelectric plate. The dimensions of the object are defined by the thickness b, width w, and length L (b <<w << L), as demonstrated in Figure. 12. Assuming that the polarization is oriented in the z direction and the x-y planes correspond to the electrodes, the extensional vibration in the x direction is represented by the dynamic equation:

$$\rho(\partial^2 u / \partial t^2) = F = (\partial X_{11} / \partial x) + (\partial X_{12} / \partial y) + (\partial X_{13} / \partial z) \qquad (21)$$

where u is the displacement of a small volume element in the ceramic plate in the x direction. When the plate is very long and thin, the longitudinal stresses, X_2 and X_3 may be set equal to zero throughout the plate, and shear stress is not generated by the electric field E_z, the necessary piezoelectric equation is reduced to:

$$X_1 = x_1 / s_{11}^{E} - (d_{31} / s_{11}^{E})\, E_z \qquad (22)$$

Therefore, the subsequent dynamic equation is obtained (it should be noted that this equation does not include a loss during vibration):

$$\rho(\partial^2 u / \partial t^2) = (1 / s_{11}^{E})(\partial^2 u / \partial x^2) \qquad (23)$$

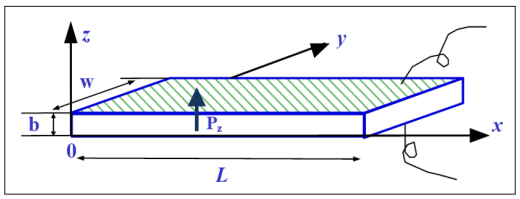

Figure 12: Longitudinal vibration specimen through the transverse piezoelectric effect (d_{31}) in a rectangular plate with dimensions of thickness b, width w, and length L (b << w << L)

The differential equation Eq. (23) is solved using the 'Laplace transform' for the transient response (We will adopt the 'Fourier transform' in the next section for analyzing the steady resonance mode). Denoting the Laplace transforms of u(t,x) and $E_z(t)$ as U(s,x) and $\tilde{E}$ (s), respectively, Eq. (23) is transformed to:

$$\rho s_{11}{}^{E} s^2 U(s,x) = \partial^2 U(s,x)/\partial x^2 \tag{24}$$

This assumes the following initial conditions:

$$u(t=0,x) = 0, \partial u(t=0,x)/\partial t = 0$$

Using $\rho\, s_{11}{}^{E} = 1/v^2$ (v: sound velocity in the piezo-ceramic), we obtain a general solution:

$$U(s,x) = A\, e^{(sx/v)} + B\, e^{-(sx/v)}. \tag{25}$$

It can be determined that the constants A and B are thus arrived at through the application of the boundary conditions. It can be demonstrated that $X_1 = 0$ at x = 0 and L. It should be noted that the strain x_1 at x = 0 and L may not require being zero, but the stress is zero:

$$X_1 = (x_1 - d_{31}E_z)/ s_{11E} = 0 \tag{26}$$

Using the fact that the strain $x_1 = \partial u/\partial x$,

$$L[x_1] = \partial U/\partial x = A\,(s/v)\, e^{(sx/v)} - B\,(s/v)\, e^{-(sx/v)}, \tag{27}$$

the boundary conditions provide the following relations to determine A and B:

$$A\,(s/v) - B\,(s/v) = d_{31}\tilde{E},$$
$$A\,(s/v)\, e^{(sL/v)} - B\,(s/v)\, e^{-(sL/v)} = d_{31}\tilde{E}$$

Consequently, Eqs. (25) and (27) become

$$U(s,x) = d_{31}\tilde{E}(v/s)[(e^{-s(L-x)/v} + e^{-s(L+x)/v} - e^{-sx/v} - e^{-s(2L-x)/v})/(1-e^{-2sL/v})], \tag{28}$$
$$L[x_1] = d_{31}\tilde{E}\left[\left(e^{-s(L-x)/v} - e^{-s(L+x)/v} + e^{-sx/v} - e^{-s(2L-x)/v}\right)/\left(1-e^{-2sL/v}\right)\right] \tag{29}$$

The inverse Laplace transformations of Eqs. (28) and (29) yield the displacement u(t,x) and the strain x_1(t,x). The fact that U(s,x = L/2) = 0 and U(s,x = 0) = − U(s,x = L) deduces u(t, x = L/2) = 0, and u(t, x = 0) = −u(t, x = L). Consequently, the total displacement of the plate device, ΔL, is equivalent to 2U(s,x = L). Thus, from Eq. (28),

$$U(s,x=L) = d_{31}\tilde{E}(v/s)\,(1-e^{-(sL/v)})\,/\,(1+e^{-(sL/v)})$$
$$= d_{31}(v/s)\tanh(sL/2v) \tag{30}$$

When $\tilde{E}$ includes the term "$(1 + e^{-(sL/v)})$," the denominator of Eq. (30) is cancelled out, leading the displacement u(t, x) is devoid of vibration ringing. However, when $\tilde{E}$ does not include the term of $(1 + e^{-(sL/v)})$, taking into account the expansion series

$$1/(1+e^{-sL/v}) = 1 - e^{-sL/v} + e^{-2sL/v} - e^{-3sL/v} \cdots\cdots$$

the strain along the x direction, x_1(t,x), is obtained by superimposing the $d_{31}E_z(t)$ curves with a specific time delay, and the ringing of the displacement will continue forever. This principle is pivotal in the elimination of superfluous vibration ringing.

Displacement Response to a Step Voltage

We consider first the most fundamental input of "Heaviside step" electric field $E(t) = E_0 H(t)$. Since the Laplace transform of the step function is given by (1/s), Eq. (30) can be expressed by

$$U(s,x=L) = d_{31}E_0(v/s^2)(1-e^{-(sL/v)})/(1+e^{-(sL/v)})$$
$$= d_{31}E_0(v/s^2)\,(1 - 2e^{-(sL/v)} + 2e^{-(2sL/v)} - 2e^{-3sL/v} + 2e^{-4sL/v}\cdots) \tag{31}$$

Note that the base function of U(s, L), $1/s^2$, gives the base function of u(t, L) in terms of t (i.e., αt). The inverse Laplace transform of Eq. (31) yields (by superposing the e^{-sk} terms):

$$u(t, L) = d_{31}E_0 v\cdot t \qquad 0 < t < L/v$$
$$u(t, L) = d_{31}E_0 v[t - 2(t - L/v)] \qquad L/v < t < 2L/v$$
$$u(t, L) = d_{31}E_0 v[t - 2(t - L/v) + 2(t - 2L/v)] \qquad 2L/v < t < 3L/v$$
$$u(t, L) = d_{31}E_0 v[t - 2(t - L/v) + 2(t - 2L/v) - 2(t - 3L/v)]$$
$$3L/v < t < 4L/v \tag{32}$$
.....

The transient displacement, ΔL (= 2·u(t, L)), produced by the step voltage is pictured in Figure 13 (since d31 is usually negative, Figure. 13 is for $E_0 < 0$). The fundamental resonance period T of this piezoelectric plate corresponds to (2L/v), and the time interval in Eq. (32) is every (T/2). Without the loss, it is noteworthy that the displacement changes linearly, as opposed to sinusoidally, an error commonly observed in the simulations of researchers. This linear displacement change is originated from the fact that the "step" function strain boundary (i.e., the boundary between the zero strain and maximum strain parts) moves with the sound velocity speed. Secondly, the overshoot is twice the magnitude of the static strain $d_{31}\, E_0\, L$.

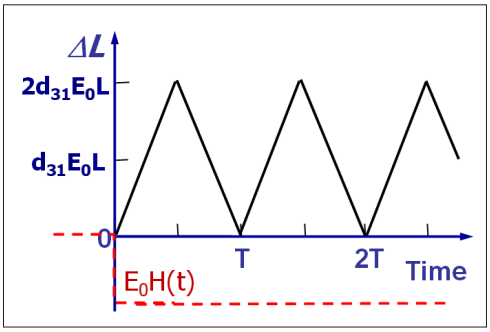

Figure 13: Triangular displacement response to a 'Heaviside step' function voltage in a continuum piezoelectric plate (d_{31} mode). The overshoot is twice the magnitude of the static strain $d_{31}E_0\, L$

Displacement Response to Pulse Drive

The response to a "rectangular pulse" voltage will be examined, as illustrated in Figuere 14(a) Top-Left corner. This control scheme is applicable to dot, inkjet printers in a direct manner. We begin by substituting.

$$\tilde{E} = \left(E_0 / s\right)\left(1 - e^{-(n\,sL)/v}\right) \quad (33)$$

into Eq. (30), which allows us to obtain the displacement ΔL for n = 1, 2 and 3. The quantity n is a time scale based on a half of the resonance period (= T/2) of the piezoelectric plate.

For n=1,

$$U(s, x=L) = d_{31}E_0\left(v/s^2\right)(1-e^{-(sL/v)})^2/(1+e^{-(sL/v)})$$

$$= d_{31}E_0\left(v/s^2\right)(1-3e^{-sL/v}+4e^{-2sL/v}-4e^{-3sL/v}+\cdots) \quad (34)$$

Similar to the 'step' case, the base function of U(s, L), $1/s^2$, gives the base function of u(t, L) in terms of t. The inverse Laplace transform of Eq. (34) yields:

$u(t, L) = d_{31}E_0 v\, t$ $\quad 0 < t < L/v$
$u(t, L) = d_{31}E_0 v[t - 3(t - L/v)]$ $\quad L/v < t < 2L/v$
$u(t, L) = d_{31}E_0 v[t - 3(t - L/v) + 4(t - 2L/v)]$ $\quad 2L/v < t < 3L/v$ (35)

.....

The transient displacement, ΔL, produced by the rectangular pulse voltage is pictured in Figure. 14(a) **Top-Right** for n=1. The resonance period of this piezoelectric plate corresponds to (2L/v). It is evident that the phenomenon exhibits continuous ringing, accompanied by an overshoot that is twice the magnitude of the static strain $d_{31}\,E_0\,L$.

For n=2,

since $\tilde{E} = (E_0 / s)(1 - e^{-(2\,Ls)/v})$ includes the denominator of Eq. (30),

$U(s,L) = d_{31}E_0(v/s^2)(1 - 2e^{-sL/v} + e\text{-}2^{sL/v})$ (36)

Thus, there is only one resonance period to analyze.

$u(t, L) = d_{31}E_0 v\, t$ $\quad 0 < t < L/v$
$u(t, L) = d_{31}E_0 v\,[t - 2(t - L/v)]$ $\quad L/v < t < 2L/v$
$u(t, L) = d_{31}E_0 v\,[t - 2(t - L/v) + (t - 2L/v)] = 0$ $\quad 2L/v < t < 3L/v$ (37)

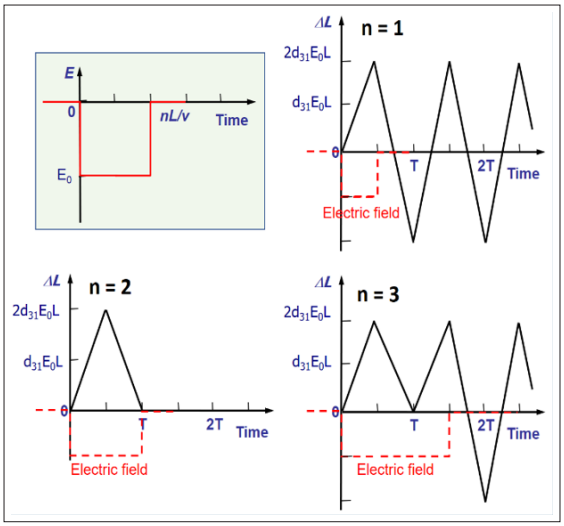

(a)

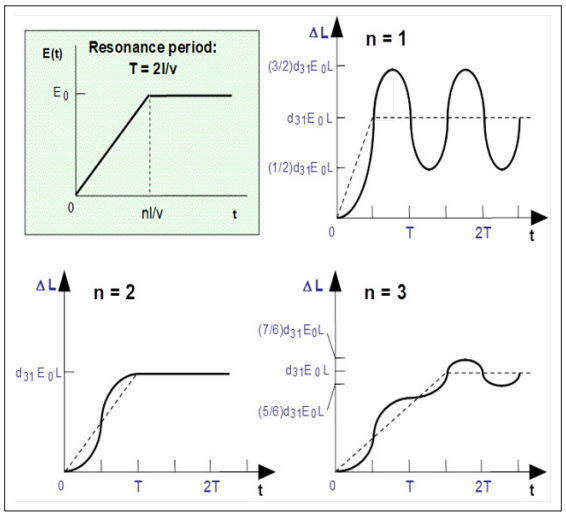

(b)

Figure 14: Transient displacement ΔL induced in a rectangular plate by a rectangular pulse voltage (a), and by a pseudo-step voltage (b). The time scale n is based on ½ of the resonance period T

In this particular instance, the displacement, designated as ΔL, transpires within the confines of a solitary pulse. This phenomenon precludes the manifestation of ringing phenomena, as illustrated in Figure 14(a) Bottom-Left. It is imperative to define the "applied field $\tilde{E}$" to incorporate the denominator term $(1 + e^{-(sL/v)})$ to ensure the realization of finite expansion terms. This will result in a one-time overshoot that is twice the magnitude of the static strain $d_{31}\,E_0\,L$. It has been demonstrated that the complete suppression of vibrational ringing can be achieved through the utilization of this method.

For n=3,

U(s, L) is again expanded as an infinite series:

$$U(s, x=L) = d_{31}E_0\left(v/s^2\right)(1-e^{-(3sL/v)})(1-e^{-(sL/v)})/(1+e^{-(sL/v)})$$

$$= d_{31}E_0\left(v/s^2\right)(1-2e^{-sL/v}+2e^{-2sL/v}-3e^{-3sL/v}+4e^{-4sL/v}-4e^{-5sL/v}\cdots) \quad (38)$$

The displacement response for this case is pictured in Figure 14(a) **Bottom-Right**. It is imperative to acknowledge that the displacement slope, delineated as the plate edge vibration velocity, manifests a twofold discrepancy between the field-applied period and the zero-field period. It has been determined that the overshoot magnitude of the ringing is twice the magnitude of the static strain $d_{31}\,E_0\,L$.

Displacement Response to Pseudo-Step Voltage

Another intriguing wave shape is the "pseudo-step," as illustrated in Figure 14(b) **Top-Left**. The drive scheme under consideration is applicable to positioning stages and cutting-edge in lathe machines. The present study commences with the substitution of

$$\tilde{E} = (E_0\, v / n\, L\, s^2)(1 - e^{-snL/v}) \quad (39)$$

into Eq. (30), we obtain the displacement ΔL for n = 1, 2, 3, ...

n = 1:

$U(s,L) = (d_{31}E_0 / L)(v^2/s^3)(1 - e^{-sL/v})^2/(1 + e^{-sL/v})$
$= (d_{31}E_0/L)(v^2/s^3)(1 - 3e^{-sL/v} + 4e^{-2sL/v} - 4e^{-3sL/v} + \cdots)$ (40)

It should be noted that the base function of U(s,L) ∝ $(1/s^3)$ corresponds to the base function of u(t,L) ∝ $(t^2/2)$, as illustrated in the following equation: Therefore, it can be concluded that the exponential term in the Laplace s domain is equivalent to the time shift in the real time domain. For instance, consider the third term in Eq. (40): $e^{-2sL/v}$, which corresponds to the time shift of 2L/v of the base u(t,L) ∝ t^2, that is, $(t - 2L/v)^2$. In each time interval:

$$u(t,L) = (d_{31}E_0v^2/2L)\, t^2 \qquad [0 < t < L/v]$$
$$u(t,L) = (d_{31}E_0v^2/2L)\, [t^2 - 3(t - L/v)^2] \qquad [L/v < t < 2L/v]$$
$$u(t,L) = (d_{31}E_0v^2/2L)\, [t^2 - 3(t - L/v)^2 + 4(t - 2L/v)^2] \qquad [2L/v < t < 3L/v] \qquad (41)$$

As illustrated in Figure 14(b) **Top-Right** panel displays the temporal variation of ΔL, defined as 2 × u(t, L), which manifests as continuous ringing. It is evident that this curve is a combination of parabolic curves, rather than a sinusoidal curve. The height of the overshoot is equivalent to ½ of $d_{31}\, E_0\, L$.

n = 2:
Now, $\tilde{E}$ includes the term $(1 + e^{-(sL/v)})$, thus,
$$U(s,L) = (d_{31}E_0\,/2L)\,(v^2/s^3)\,(1 - 2e^{-sL/v} + e^{-2sL/v}) \qquad (42)$$

Thus,
$$u(t,L) = (d_{31}E_0v^2/4L)\, t^2 \qquad [0 < t < L/v]$$
$$u(t,L) = (d_{31}E_0v^2/4L)\, [t^2 - 2(t - L/v)^2] \qquad [L/v < t < 2L/v]$$
$$u(t,L) = (d_{31}E_0v^2/4L)\, [t^2 - 2(t - L/v)^2 + 4(t - 2L/v)^2]$$
$$= d_{31}E_0\, 2/L \qquad [2L/v < t] \qquad (43)$$

As demonstrated in Figure 14(b) **Bottom-Left**, ΔL does not demonstrate ringing. The application of the field $\tilde{E}$ is indicated by the term "$(1 + e^{-(sL/v)})$" included. The expansion series terminates in finite terms, leading to complete suppression of both overshoot and subsequent vibrational ringing.

As demonstrated in Figure 14(b) **Bottom-Left**, ΔL does not demonstrate ringing. The application of the field $\tilde{E}$ is indicated by the term "$(1 + e^{-(sL/v)})$" included. The expansion series terminates in finite terms, leading to complete suppression of both overshoot and subsequent vibrational ringing.

For n = 3,
The U(s,L) expansion is subject to further infinite expansion, thereby resulting in a state of perpetual ringing. As illustrated in Figure 14(b) **Bottom-Right**, the displacement-time relationship is depicted in the lower right quadrant. It is imperative to reiterate that all the curves under consideration are composed of parabolic curves, and the height of the overshoot is equivalent to 1/6 of $d_{31}E_0L$. In the case of n = 4, the ringing can once again be eliminated through the conceptualization of the denominator of Eq. (30) as being indistinguishable.

Reminder: When electric field, $\tilde{E}$ under consideration includes the term '$(1 + e^{-(sL/v)})$', the denominator of the Laplace form of displacement, U(s,x=L) is cancelled. As Eq. (30) becomes a finite-term equation, the displacement u (t, x) is not accompanied by the phenomenon of vibration ringing. The following empirical process is proposed to effectively suppress overshoot and ringing: (1) By applying a relatively steep "step" voltage to the actuator, the resonance period can be obtained as the time period between the overshoot peak and the successive peak point. (2) Then, by adjusting the voltage rise time with precision to the resonance period to ensure the elimination of overshoot and ringing of the vibration on subsequent occasions. This vibration ringing suppression technique does not fall into the categories of passive vibration damping, which involves the dissipation of energy through Joule heat, or active vibration damping, which involves the external application of power to counteract mechanical vibrations.

MECHANICAL IMPEDANCE MATCHING

Question 8(a): According to the assertion of an engineer specializing in medical technology, the utilization of PZT, characterized by its elevated electromechanical coupling factor, k, is optimal for piezoelectric sensors intended for heartbeat monitoring applications. What are the flaws in this concept?

Question 8(b): In order to mitigate a particular mode of vibration in an aluminum cantilever beam, a mechanical engineer employs a shunted soft-piezoelectric composite (Macro Fiber Composite manufactured by Smart Material Corp., FL) bonded to the beam, as illustrated in Figure 15. From the perspective of mechanical and acoustic impedance matching, this design is suboptimal. The reader is requested to thoroughly discuss the problems, then, to propose an alternative design to significantly enhance piezoelectric damping performance.

Solution: Mechanical energy transmission and electromechanical energy transduction rate are considered for the piezoelectric damping performance.

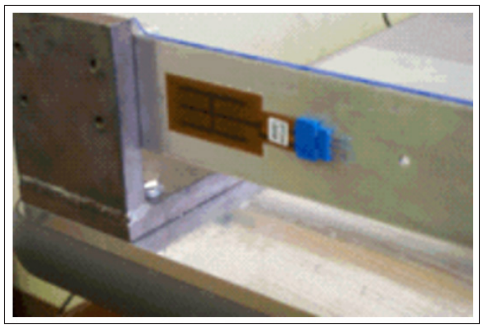

Figure 15: Vibration damping of a single mode vibration of an aluminum cantilever beam using a piezoelectric composite bonded on the beam

Mechanical Impedance Matching

The mechanical work transferred from one object to another is determined by the product of the applied force, F, and the displacement, L, of the interface.:

$$W = F \cdot \Delta L$$

As illustrated in Figure 16(a), a conceptual cartoon is employed to demonstrate two extreme cases. In the event that the object is of a very soft nature, the force F can be miniscule, resulting in a correspondingly negligible W (effectively no work) [3,22]. This phenomenon is analogous to the proverb known as "Pushing a curtain," which is exemplified by the case when the acoustic wave is generated in water directly by a hard PZT transducer. The majority of the acoustic energy generated in the PZT is reflected

at the interface, with only a negligible amount of acoustic energy transferring into water. Conversely, in the event that the object is of considerable hardness, the displacement will be negligible, resulting in a correspondingly negligible W. This phenomenon is analogous to the proverb of "pushing a wall." As demonstrated in Figure 15, polymer piezoelectric PVDF (polyvinylidene fluoride) or soft MFC is incapable of efficiently driving a hard metal part. Therefore, the 'mechanical/acoustic impedance' $Z = \sqrt{\rho c}$ must be adjusted to maximize the output mechanical power:

$$\sqrt{\rho_1 c_1} = \sqrt{\rho_2 c_2} \tag{44}$$

where ρ is the density and c is the elastic stiffness, and the subscripts 1 and 2 denote the two materials. This is one of the key factors for developing piezoelectric energy harvesting systems. In medical array transducers, acoustic impedance matching layers are fabricated on the PZT transducer to optimize the transfer of mechanical energy to water (see Figure 16(b)). These layers consist of elastically intermediate materials between PZT and water, such as a polymer. To be more precise, the matched acoustic impedance Z should be selected as follows: $\sqrt{Z_1 \cdot Z_2}$). The geometric average is calculated as follows: where Z_1 and Z_2 represent the acoustic impedances of PZT and human tissue (which approximate that of water), respectively. This finding resolves Question 8(a) by demonstrating that the absence of an acoustic impedance matching layer results in a scenario where the acoustic wave generated in the PZT is reflected at the interface without transmitting to water.

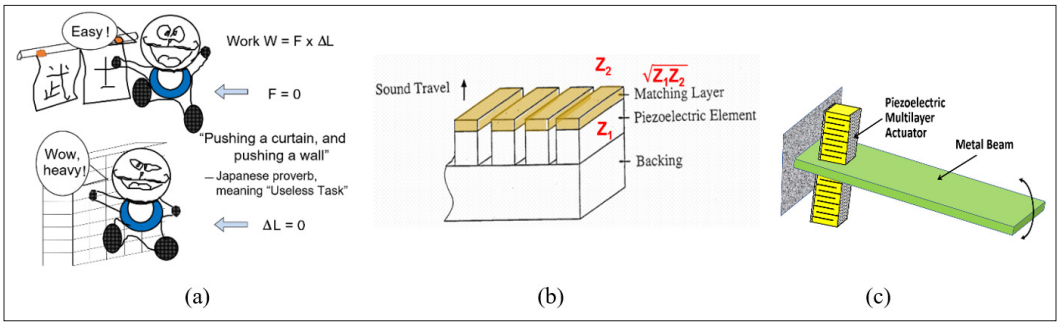

Figure 16: (a) Conceptual illustrations of mechanical impedance matching. "Pushing a curtain, pushing a wall." (b) Medical imaging array transducer assembly with acoustic impedance matching layer. (c) Ideal vibration damping structure of a metal beam

Vibration Damping and Electromechanical Coupling

The unimorph piezoelectric element shown in Figure 15 is a typical example of a combination of a vibration object and a piezoelectric material. The cantilever beam is hit by a mechanical impulse force, and the transient vibration displacement decay is monitored by a non-contact displacement sensor.

Let us evaluate the damping constant theoretically [23,24]. The electric energy U_E generated can be expressed by using the electromechanical coupling factor k and the input mechanical energy U_M from the vibration cantilever beam:

$$U_E = U_M \times k^2 \tag{45}$$

The piezoelectric damper transforms electric energy into heat energy when the external impedance R is connected, and transforming rate of the damper can be raised to a level of up to 50% when the electrical impedance is matched. That is, the external resistance R should be adjusted to $1/\omega C$, where C is the capacitance of the piezo-transducer. Accordingly, the vibration energy is transformed at a rate of $(1 - k^2/2)$ times with energy vibration repeated, since $k^2/2$ multiplied by the amount of mechanical vibration energy is dissipated as heat energy. As the square of the amplitude is equivalent to the amount of energy, the amplitude undergoes a decrease at a rate of $(1-k^2/2)^{1/2}$ with each successive vibration. Assuming the resonance period is designated as T_0, the number of vibrations for a time period t (sec) is calculated as $2t(sec)/T_0$. Therefore, the amplitude in t sec is as follows: $(1-k^2/2)^{t/T_0}$). If the residual vibration period is taken to be T_0, the damping in the amplitude of vibration in t sec can be expressed as follows:

$$(1-k^2/2)^{t/T_0} = e^{-t/\tau} \tag{46}$$

Thus, the following relationship for the time constant τ of the vibration damping is obtained.

$$\tau = -\frac{T_o}{\ln(1-k^2/2)} \tag{47}$$

Given that the researcher employed a unimorph structure in the study in Figure 15, presumably due to its simplicity, it is not feasible to anticipate adequate damping performance, given the negligible electromechanical coupling factor, k, the percentage of which is less than 10%. The multilayer (ML) PZT actuators with $k_{33} = 70\%$ will be a better alternative choice for this system. As illustrated in Figure 16(c), two ML actuators can sandwich the aluminum beam around the cantilever supporting nodal part, then the other ends of the ML actuators should be rigidly supported on the beam-clamping walls. Since the ML actuator has a similar mechanical impedance to the vibrating metal beam, mechanical energy transfer from the beam to the ML devices is smooth. Furthermore, due to the PZT volume in the ML much larger than the MFC composite, handling energy level will be sufficient to this large beam vibration in the level of mechanical energy ~10 W/cm^3.

Reminder: The act of acoustic impedance ($Z = \sqrt{\rho c}$) matching is analogous to the proverb, "Pushing a curtain and pushing a wall." It is imperative to consider the mechanical and acoustic impedance matching of the actuators to facilitate the effective transfer of mechanical energy from both material and structural perspectives.

PIEZOELECTRIC ENERGY HARVESTING

Question 9: The present study was conducted with the objective of identifying research trends that emerged subsequent to the 2000s. This investigation was informed by a comprehensive review of the relevant literature, which included a detailed examination of a specific book Ref. [25]. Uchino, a leading figure in the field of piezoelectric energy harvesting, has expressed a sense of frustration with the majority of recent research papers. This sentiment is rooted in certain observations and concerns, which are outlined below:

(1) Despite the fact that the electromechanical coupling factor, k, is minimal (i.e., the energy conversion rate from the input mechanical to electric energy is the lowest) among the various device configurations, the majority of researchers primarily utilize the "unimorph" or "bimorph" design. Why?
(2) Despite the standard noise vibration operating within a considerably lower frequency range, researchers have measured the amplified resonant response (even at frequencies exceeding 1 kHz) and documented these unrealistically harvested electric energies in their respective papers. Why?
(3) Despite the harvested energy being lower than 1 mW, which is lower than the required electric energy to operate a typical energy harvesting electric circuit with a DC/DC converter (typically around 2 – 3 mW), the researchers report the result as an energy 'harvesting' system. Why? It is imperative to ascertain whether this scenario signifies a genuine loss of energy.

(4) A paucity of literature has documented the complete energy flow or precise efficiency from the input mechanical noise energy to the final electric energy in a rechargeable battery via the piezoelectric transducer in a step-by-step manner. Why? In comparison with commercially available photovoltaic cells that exhibit efficiencies ranging from 5% to 9%, customers of piezoelectric energy harvesting devices can anticipate efficiencies within a similar range.

The predominant response from these researchers to the aforementioned inquiries, "why?", is an assertion that the rationale underpinning their approach is rooted in the methods of preceding researchers: "because the preceding researcher did so!" The development of enhanced strategies to address the aforementioned inquiries is imperative.

Solution: In the 21st century, piezoelectric energy harvesting has become a subject of interest in research communities, particularly in the context of sustainability and renewable energy. The author's pioneering work in the field of piezoelectric damping technology, initiated in the 1980s, was aimed at mitigating engine noise vibration. However, following the 1990s, the phenomenon of a rechargeable battery accumulating electric charge from the vibrations in the environment without the consumption of the electric field has been observed [26]. "Lightning Switch" [26] (remote switch for room lights, with using a unimorph piezoelectric component) by PulseSwitch Systems, VA is one of the successful million-selling products in the commercial market. In addition to the living convenience, Lightning Switch can reduce the housing construction cost. Another successful product is the "PABM," a 25 mm caliber "Programmable Air-Burst Munition" developed by ATK, AZ, and Micromechatronics, PA [26]. This munition employs a multilayer (ML) piezo-actuator to generate electric energy during the shot impact, which subsequently activates the operational amplifiers, leading to the burst according to the command program.

The author expresses enthusiasm regarding the significant surge in research publications within this domain. However, he also conveys a sense of embarrassment upon encountering publications of a frivolous nature, such as the following:

- The energy harvesting process from a hard steel structure with a soft piezo-material results in a mechanical impedance mismatch.
- The process of energy harvesting from a high-frequency (100 kHz) resonant state in the MEMS devices is not applicable to natural noise, which operates at a frequency that is much lower than this frequency level.
- The energy harvesting from the MEMS structure is found to be inadequate, with a mere nW~μW recorded. This deficiency is further compounded by the harvesting circuit's substantial energy consumption, measured in mW.

The author delineates the preliminary research guidelines and elucidates the challenges and limitations associated with the implementation of the piezoelectric transducer. The Penn State University group developed energy harvesting piezoelectric devices based on a "cymbal" structure (29 mm diameter × 1–2 mm thick), which can generate electric energy up to 100 mW under an automobile engine vibration [27,28]. A washer-like energy harvesting sheet was developed for a hybrid car application, aiming at 1 W-level constant accumulation from the engine vibration to a fuel cell. This was accomplished by combining three cymbals in a rubber composite. As illustrated in Figure 17 [26], the process of piezoelectric energy harvesting is comprised of three primary phases or steps: (i) "mechanical-mechanical energy transfer," which encompasses the mechanical stability of the piezoelectric transducer under substantial stresses and mechanical impedance matching; (ii) "mechanical-electrical energy transduction." The subject of this investigation is the electromechanical coupling factor in the composite transducer structure, as indicated in the following Section 2.9.2; and (iii) "electrical-electrical energy transfer," which includes electrical impedance matching, such as a DC/DC converter to accumulate the energy into a rechargeable battery.

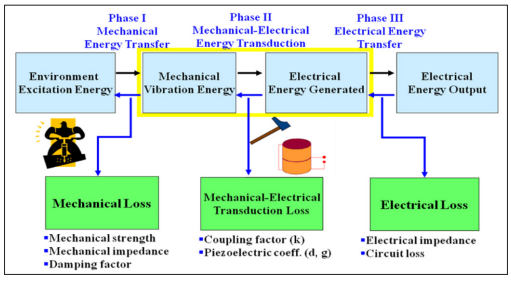

Figure 17: Three primary phases associated with piezoelectric energy harvesting. The transfer of energy may occur in three distinct ways: (i) mechanical-mechanical energy transfer, (ii) mechanical-electrical energy transduction, and (iii) electrical-electrical energy transfer

To that end, the subsequent section will examine the decrease in energy amount that occurs during successive transmitting and

transducing phases. This examination will be conducted through the utilization of numerical analyses derived from Figure 18. The specimen employed in this study is a cymbal with 0.3 mm-thick stainless-steel endcaps, which was inserted beneath a 4 kg engine weight (i.e., 40 N bias force). The electromagnetic shaker was operated at 100 Hz (i.e., the actual engine noise frequency) for a period of 8 seconds, and the accumulated energy during that time period was measured at each point.

Source to Transducer: Mechanical Impedance Mismatch

8.22 J/9.48 J = 87% of the mechanical energy is transmitted from the source to piezo-cymbal transducer. It is imperative to take the mechanical impedance of the transducer into consideration, as it significantly impacts the efficiency of mechanical energy transfer. In instances where the mechanical impedance is not adequately addressed, a substantial portion of energy is reflected at the contact or interface point, leading to inefficient energy conversion.

Transduction in the Transducer: Electromechanical Coupling

Transduction rate is evaluated by k^2. Since the k_{eff} = 0.25~0.30 in the cymbal, the energy conversion rate will be 9% maximum. The remaining portion will remain as the original mechanical vibration energy. 0.74 J/8.22 J = 9.0%. Given that the bimorph or unimorph is characterized by a significantly smaller electromechanical coupling factor, ranging from 10% to 15%, the energy conversion rate is found to be less than 2%. The utilization of transducer modes with elevated k values is strongly advised.

Transducer to Harvest Circuit: Electrical Impedance Matching

The ratio of 0.42 J/ 0.74 J = 57% is indicative of an electrical impedance mismatch between the cymbal output and the circuit input. The AC/DC rectifying circuit is the primary contributor to a half cut.

Harvesting Circuit to Rechargeable Battery

0.34 J/0.42 J = 81%. This reduction is attributable to two factors. Firstly, it is due to the energy consumption in the circuit. Secondly, it is due to the electrical impedance mismatch between the circuit output (which remains at approximately 5 kΩ) and the rechargeable battery impedance (which is approximately 10-20 Ω). It has been determined that, given the standard consumption of a circuit of 1–3 mW, energy harvesting at levels below this range is rendered ineffective.

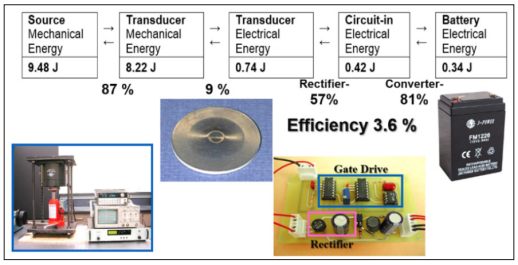

Figure 18: Energy flow analysis from the vibration source, through the piezoelectric element, then via energy harvesting circuits, to finally into a rechargeable battery

As previously mentioned, the primary issue in piezoelectric energy harvesting is the low electromechanical coupling factor employed by researchers. The adoption of the ML-type actuator is imperative. It can be demonstrated that k_{33} is equivalent to 50%. This finding suggests that the efficiency can be enhanced by a factor of 10. For a more thorough examination of high-energy conversion designs, please refer to Figure 19.

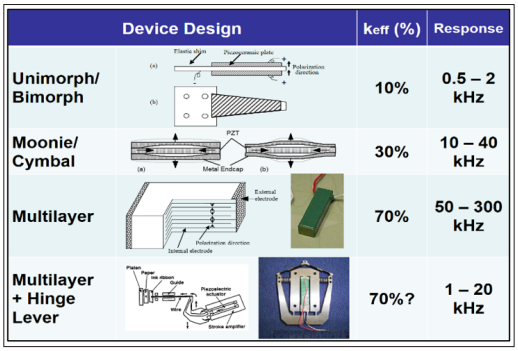

Figure 19: Promising piezoelectric device designs for energy harvesting applications. In comparison with unimorph or bimorph designs, ML actuators are shown to enhance the energy harvesting rate by two orders of magnitude

Reminder: It is not advisable to employ unimorph or bimorph configurations in the piezo-energy harvesting system, as this approach yields a lowest electromechanical coupling factor k value. It is imperative to refrain from disputing the energy harvesting process at the resonance frequency of the piezoelectric component, as this would constitute an unrealistic value. The current energy harvesting rate from the vibration source engine to the storing battery is 3.6%, which is comparable to solar cell devices. It is imperative to consider losses in all the aforementioned phases to enhance the system's efficiency. The utilization of a high k such as multilayer designs is strongly recommended. With respect to the MEMS energy harvesting researchers, it is requested that the research be focused on the development of two methods: (1) Utilization of a substantial PZT film > 30 μm, (2) Parallel arrangement of numerous μW components, which exhibits a synchronous connection that culminates in an electrical energy output of 1 mW. This level of energy is deemed pragmatic, as it is within the realm of practical implementation and utilization.

RESONANCE & ANTIRESONANCE MODES

Question 10: In the field of materials engineering, the resonance mode is widely regarded as a particular manifestation of mechanical resonance. Conversely, the antiresonance mode is not regarded as a mechanical resonance because the displacement amplitude of a piezoelectric specimen augments solely at its resonance frequency, not at the antiresonance frequency, when it is driven "under constant voltage." Alternatively, the resonance mode is regarded as the most efficient driving condition for the piezoelectric transducer. It is imperative to ascertain whether the reader is able to discern that the aforementioned two claims have been derived from misconceptions regarding piezoelectricity.

Solution: The resonance/antiresonance vibration modes are basically sinusoidal, and we use "Fourier transform," rather than Laplace transform, for the continuous and steady vibration analysis. We proceed to deliberate on the longitudinal mechanical vibration of a piezoceramic plate through the transverse piezoelectric effect (d_{31}), as illustrated in Figure 12. In the event that the polarization is oriented in the z-direction

and the x-y planes correspond to the electrodes, the extensional vibration in the x direction is depicted by Eq. (23). When the length L exceeds 4 to 6 times the width w or the thickness b, the coupling modes involving width or thickness vibrations can be disregarded, resulting in a harmonic vibration [3].

$$-\omega^2 \rho s_{11}^{E} u = \partial^2 u / \partial X^2 \tag{48}$$

Here, ω is the angular frequency of the drive field, and ρ is the density. Substituting a general solution $u=u_1(x)e^{j\omega t} + u_2(x)e^{-j\omega t}$ into Eq. (48), and with the boundary condition $X_1 = 0$ at x = 0 and L (sample length) (due to the mechanically-free condition at the plate end), the following solution can be obtained:

$$\partial u / \partial x = x_1 = d_{31} E_z [\sin \omega (L-x)/v + \sin(\omega x / v)] / \sin(\omega L / v)$$
$$= d_{31} E_z \left(\frac{\cos\left[\frac{\omega(L-2X)}{2V}\right]}{\cos\left(\frac{\omega L}{2V}\right)} \right) \tag{49}$$

where *v* is the 'sound velocity' of the piezoelectric plate along the x axis expressed by $v = 1/\sqrt{\rho s_{11}^{E}}$

It is imperative to acknowledge that both resonance and antiresonance modes constitute instances of 'mechanical resonance.' However, electrical engineers concentrate on the electrical impedance (applied voltage/induced current) ratio or admittance from the electric drive system viewpoint. The present influx of current into the specimen is delineated by the surface charge increment, $\frac{\partial D_3}{\partial t}$, and the aggregate current is expressed as follows:

$$I = j\omega w \int_0^L D_3 dx = j\omega w \int_0^L (d_{31} X_1 + \varepsilon_0 \varepsilon_{33}^{X} E_z) dx$$
$$= j\omega w \int_0^L [d_{31} x_1 / s_{11}^{E} - (d_{31} / s_{11}^{E}) E_z + \varepsilon_0 \varepsilon_{33}^{X} E_z] dx \tag{50}$$

Using Eq. (50), the admittance Y for the mechanically free sample is calculated to be:

$$Y = (i/V) = (i/E_z b)$$
$$= (j\omega w L / E_z b) \int_0^L \left[(d_{31}^2 / s_{11}^{E}) \left(\frac{\cos\left[\frac{\omega(L-2x)}{2V}\right]}{\cos\left(\frac{\omega L}{2v}\right)} \right) E_z + \left[\varepsilon_0 \varepsilon_{33}^{X} - (d_{31}^2 / s_{11}^{E}) \right] E_z \right] dx$$
$$= (j\omega w L / b) \varepsilon_{33}^{LC} \left[1 + (d_{31}^2 / \varepsilon_{33}^{LC} s_{11}^{E}) (\tan(\omega L / 2V) / (\omega L / 2V)) \right] \tag{51}$$

In this configuration, the variable w denotes the width of the rectangular piezoelectric sample, L is the length, b is the thickness, and V is the applied voltage. The longitudinal clamped sample's permittivity, ε_{33}^{LC}, is calculated using the following equation (refer to the argument in Question 4):

$$\varepsilon_0 \varepsilon_{33}^{LC} = \varepsilon_0 \varepsilon_{33}^{X} - \left(\frac{d_{31}^2}{s_{11}^{E}} \right) = \varepsilon_0 \varepsilon_{33}^{X} (1 - k_{31}^2) \tag{52}$$

Resonance & Antiresonance Modes

The phenomenon of "piezoelectric resonance" is achieved when the admittance reaches an infinite value or the impedance becomes zero, a condition that is achieved by neglecting the losses associated with the material. Therefore, the resonance frequency of f_R is calculated from ωL/2v=π/2 in Eq. (51), because tan(ωL/2v) → ∞ for ωL/2v→π/2. The fundamental frequency is expressed as

$$f_R = \omega_R / 2\pi = v / 2L = 1 / 2L\sqrt{\rho s_{11}^{E}} \tag{53}$$

Conversely, the antiresonance state is generated under the condition of zero admittance or infinite impedance. By putting Y = 0 in Eq. (51):

$$(\omega_A L / 2v) \cot(\omega_A L / 2v) = -d_{31}^2 / \varepsilon_{33}^{LC} s_{11}^{E} = -k_{31}^2 / (1 - k_{31}^2) \tag{54}$$

The final transformation is provided by the electromechanical coupling factor definition,

$$k_{31} = d_{31} / \sqrt{s_{11}^{E} \cdot \varepsilon_0 \varepsilon_{33}^{X}} \tag{55}$$

The mode difference between the resonance and antiresonance states can be described by the following model, which is intended to serve as an intuitive guide. In a high electromechanical coupling material with k_{31} almost equal to 1, resonance or antiresonance states emerge for tan(ωL/2v) = ∞ or 0. That is to say, ωL/2v is equivalent to (m−1/2) π or m π (m: integer), respectively. The strain amplitude x_1 distribution for each state [calculated using Eq. (49)] is illustrated in Figure 20. In the resonance state, large strain amplitudes and associated large capacitance changes (called 'motional capacitance') are induced, and the current can easily flow into the device (i.e., large admittance). Conversely, at the antiresonance, the strain induced in the device compensates entirely (due to one wavelength), resulting in no dynamic/motional capacitance change, and the current cannot flow easily into the sample. Thus, for a high k material the first antiresonance frequency f_A should be twice as large as the first resonance frequency f_R. It is noteworthy that the maximum strain level is equivalent for both the resonance and antiresonance modes.

It is hypothesized that the stress at the plate ends (x = 0 and L) will be equivalent to zero in both cases. However, while the strain x_1 at the plate ends approaches a value of zero for the resonance, the strain x_1 does not equal zero for the antiresonance. Therefore, it can be concluded that a single vibration node is present at the center of the plate for the resonance (see Top-Left of Figure 20), while two additional nodes are observed at the plate's extremities for the antiresonance (see Top-Right of Figure 20). This configuration corresponds to a value of k_{31} equal to 1. The magnitude of the end displacement is negligible, while the internal plate displacement is substantial.

In a practical PZT case with k_{31} = 0.3, the antiresonance state varies from the previously mentioned mode and becomes closer to the resonance mode (Top-Center of Figure 20). The material under consideration exhibits an antiresonance mode, in which the capacitance change due to size change (i.e., "motional capacitance") is completely compensated by the current required to charge the static capacitance (i.e., "damped capacitance"). Therefore, it can be deduced that the antiresonance frequency of f_A will approximate the resonance frequency of f_R. It has been demonstrated that the displacement at the plate ends is nearly equivalent to the maximum (anti-node) point when k_{31} is small.

Despite the fact that both the resonance and antiresonance states are classified as mechanical resonance, the misconception that "antiresonance is not a mechanical resonance" arises from the observation that no displacement enhancement is detected under a "constant voltage drive." It has been observed that when the antiresonance state exhibits high impedance, the current flow is minimal (i.e., a very low input electric power), resulting in low mechanical excitation. In the event that the experiment is conducted under the parameters of a "constant current drive," a substantial voltage is applied at the anti-resonance point. This results in a significant increase in power input, which consequently leads to the attainment of the peak vibration level.

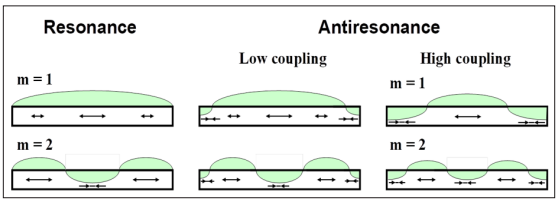

Figure 20: Strain distribution in the resonant and antiresonant states in the k_{31}-type plate

In order to verify the mechanical resonance of the antiresonance mode, the "mechanical excitation" of this mode is explained by means of a burst/transient method [29,30]. The "burst method" involves subjecting the piezoelectric material to a predetermined number of AC (near resonance) voltage cycles. Following this excitation, the material is electrically shut down, resulting in either a short-circuit condition (i.e., resonance under electrical excitation) or an open-circuit condition (i.e., antiresonance under electrical excitation). These conditions are maintained on the sample to observe the "mechanical" decaying AC vibration without the need for electrical power input, as illustrated in Figure 21. It is noteworthy that the vibration amplitude and velocity at the plate ends are directly proportional to the current and voltage generated in the piezo-ceramic at the resonance or antiresonance mode, respectively. It is imperative to observe the resonance frequency jump that occurs under open-circuit conditions, as illustrated in Figure 21(b). This occurrence signifies an increase in elastic stiffness when the open-circuit is generated from the initial short-circuit. The decay of current or voltage allows for the calculation of the mechanical quality factors at resonance Q_A and antiresonance Q_B, respectively, as a function of vibration velocity, an important figure of merit for high power applications (this methodology will be used in the next Subsection 2.10.2). It is imperative to emphasize that the mechanical resonance frequency in the vibration velocity monitoring abruptly shifts exclusively under the open-circuit condition. That is to say, the natural "mechanical antiresonance" mode is induced subsequent to the burst resonance mode drive.

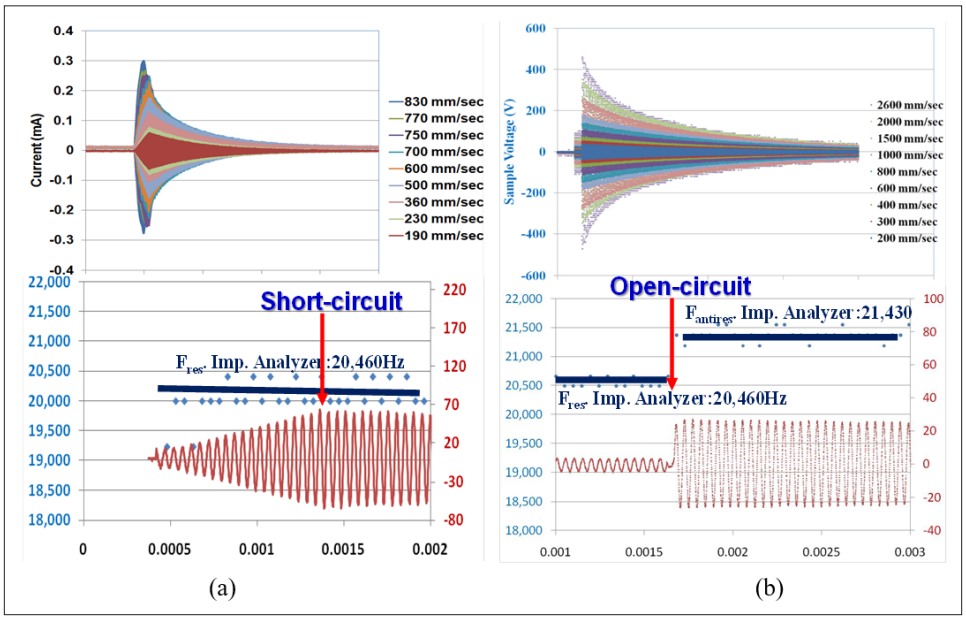

Figure 21: (a) Burst methods under short-circuit condition, where current and vibration velocity change proportionally; (b) Burst methods under open-circuit condition, where voltage and vibration velocity change proportionally. Note the resonance frequency jump to the antiresonance frequency for the open-circuit

Heat Generation at Antiresonance Mode

High-power piezoelectrics with low loss have emerged as a central research topic from the energy-efficiency improvement viewpoint. That is to say, the research focus is shifting from "real (off-resonance strain magnitude)" to "imaginary performance (heat generation reduction)." From the perspective of transducer application, the primary objective is to minimize hysteresis and enhance the mechanical quality factor to amplify the "resonance displacement." The piezoelectric properties of a material undergo alterations due to its non-linear characteristics and hysteresis, which manifest under conditions of high excitation. High Power Characterization System (HiPoCS™) was developed in the ICAT at the Penn State University to fill the void between initial property measurements under small vibration velocity and actual service conditions under high vibration velocity with heat generation [30]. HiPoCS is a system that has been developed for the purpose of measuring high-power characteristics and replicating the service conditions of piezoelectric materials under constant voltage (V_{rms}), current (A_{rms}), vibration velocity (V_{rms}), and input electrical power (P) modes. It has been demonstrated that prior measurements conducted under constant voltage or current modes are inadequate in providing the precise mechanical quality factors Q_A and Q_B from the admittance/impedance curves. This limitation arises due to the presence of

significant distortion (i.e., skewed shape) in the spectra, which is attributed to the elastic non-linearity inherent in piezo-ceramics. Consequently, the most significant advancement in high-power measurement was achieved through the implementation of the "constant vibration velocity" mode in HiPoCS. In this mode, the material's stored mechanical energy level is kept constant throughout the measurement so that the elastic nonlinearities and thus-associated admittance spectrum distortions in property calculations can be avoided.

It is hypothesized that the resonance and antiresonance modes are proximate for small values of k_{31}, as illustrated in Figure 22(a), the case demonstrates the voltage and current characteristics in the frequency sweep from the resonance to the antiresonance points under "constant vibration velocity" with HiPoCS, measured on a PZT ceramic. Using the 3 dB up method for the voltage or current curve, the mechanical quality factor at resonance Q_A or at antiresonance Q_B can be obtained. It is obvious that the apparent power (the product voltage & current) is smaller at the antiresonance than the resonance under the same output vibration level; that is, the efficiency is higher at the antiresonance than the resonance in the PZTs. The motivation behind Uchino's endeavor to elucidate the mechanisms of loss emerged in the late 1980s, when he became cognizant of the substantial Q_M discrepancy between the resonance and antiresonance in PZT ceramics. This discrepancy could not be explained by the prevailing IEEE Standard measuring method at the time.

In order to elucidate the physical underpinnings that give rise to the antiresonance mechanical quality factor exceeding that of resonance, a concise exposition of loss phenomenology is herein introduced. Refer to Ref. [31] for a more thorough discussion. In the context of piezoelectrics, three distinct losses must be considered: dielectric *tanδ*, elastic *tanφ* and *tanθ*, are further categorized into two distinct types: intensive losses, which are observable in nature, and extensive losses, which are associated with the material parameters of the system under investigation. The categorization of losses is delineated by the following definitions:

$\varepsilon^{X*}= \varepsilon^{X}(1-j\tan\delta')$, $s^{E*} = s^{E}(1-j\tan\varphi')$, $d^{*} = d(1-j\tan\theta')$;
$\kappa^{x*} = \kappa^{x}(1+j\tan\delta)$, $c^{D*}=c^{D}(1+j\tan\varphi)$, $h^{*}=h(1+j\tan\theta)$

Intensive (prime) and extensive (non-prime) losses correspond to the 'stress-free or short-circuit' status and the 'clamped or open-circuit' status, respectively. Furthermore, the intensive and extensive loss factors have the following relationship for the k_{31} mode:

$$\begin{bmatrix}\tan\delta'\\ \tan\varphi'\\ \tan\theta'\end{bmatrix} = K\begin{bmatrix}\tan\delta\\ \tan\varphi\\ \tan\theta\end{bmatrix} or \begin{bmatrix}\tan\delta\\ \tan\varphi\\ \tan\theta\end{bmatrix} = K\begin{bmatrix}\tan\delta'\\ \tan\varphi'\\ \tan\theta'\end{bmatrix} \quad (56)$$

Here, the conversion matrix K is defined in terms of the electromechanical coupling factor k as;

$$k = \frac{1}{1-k^2}\begin{pmatrix}1 & k^2 & -2k^2\\ k^2 & 1 & -2k^2\\ 1 & 1 & -1-2k^2\end{pmatrix}\left(k = d/\sqrt{\varepsilon_0\varepsilon^X\cdot s^E}\right) \quad (57)$$

The matrix K is proven to be 'involutory,' i.e., $K^2 = I$, or $K = K^{-1}$, where I is the 'identity matrix.'

We derived the formula of Q_A and Q_B in terms of the three loss factors for various vibration modes in Refs. [31] and [32]. In the case of the k_{31}-type plate, for instance:

$$\frac{1}{Q_{A,31}} = \tan\varphi_{11}', \; or \; Q_{A,31} = \frac{1}{\tan\varphi_{11}'} \quad (58a)$$

$$\frac{1}{Q_{B,31}} = \frac{1}{Q_{A,31}} - \frac{2}{1+\left(\frac{1}{K_{31}}-K_{31}\right)^2\Omega_{B,31}^{\;2}}(2\tan\theta_{31}' - \tan\delta_{31}' - \tan\varphi_{31}') \quad (58b)$$

Here, $\Omega_{B,31} = \frac{\omega_B^{\,L}}{2V_{11}^E}$ is the normalized antiresonance frequency based on ω_B. It is imperative to consider the factors, $k^2=d^2/\varepsilon_0\,\varepsilon^X s^E$, to comprehend the term $(2\tan\theta_{31}'-\tan\delta_{33}'-\tan\varphi_{11}')$ as the "electromechanical coupling loss", that is a specific designation used to describe a particular phenomenon. Though previous researchers had overlooked the significance of piezoelectric loss $\tan\theta_{31}'$, Uchino's group demonstrated that piezoelectric loss possesses the most substantial magnitude in comparison with dielectric and elastic losses in PZT compositions. This finding is crucial for comprehending the admittance/impedance spectrum. In order to elucidate the phenomenon of $Q_A < Q_B$ in PZTs, it is imperative to consider the piezoelectric loss as being of greater magnitude than the mean of the other dielectric and elastic losses (i.e., $\tan\theta_{31}' > \frac{1}{2}(\tan\delta_{33}' + \tan\varphi_{11}')$). It is important to note that the empirical rule $Q_A < Q_B$ does not always hold true for the Pb-free piezoelectrics. Figure 22(b) demonstrates the heat generation profiles on a Hard PZT specimen for the resonance (Type A) and antiresonance (Type B) under the same vibration level drive (i.e., "vibration velocity constant"). Under v_{rms} = 0.55 m/sec, the maximum temperature at the nodal point (60°C) under the antiresonance is much lower than that under the resonance (95°C), as expected from $Q_A < Q_B$.

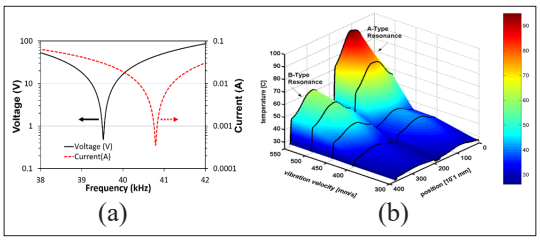

(a) (b)

Figure 22: (a) Voltage and current characteristics in the frequency sweep from the resonance to the antiresonance frequency under constant vibration velocity with HiPoCS, conducted on a PZT ceramic. (b) Heat generation profiles for the resonance (Type A) and antiresonance (Type B) under the same vibration velocity on a hard PZT (APC 851) with HiPoCS [30,32]

Reminder: In PZTs, the antiresonance mode has been demonstrated to exhibit superior efficiency (lower heat generation) in comparison to the resonance mode when generating equivalent mechanical output in transducer applications. The fundamental distinction between the two lies in the drive scheme employed: a high voltage, low current drive is utilized for antiresonance, while a low voltage, high current drive is employed for resonance.

It is noteworthy to mention the recent studies by Shekhani et al., entitled "Evaluation of the Mechanical Quality Factor under High Power Conditions in Piezoelectric Ceramics from Electrical Power" [33], yielded the highest Q_M (greater than Q_A, Q_B) at a specific frequency f_M between f_A and f_B. The intermediate voltage and current are employed to regulate the equivalent vibration level while maintaining minimal electric energy.

SYSTEM DESIGN PRINCIPLE

Question 11: The predominant tendency among industrial device developers is to prioritize the development of "components," often by acquiring the driving circuit from the manufacturer to minimize expenses and the duration of development. From the perspective of straightforward device development, the "component-purchasing" approach is a viable strategy. Nevertheless, when assessed from the perspective of sophisticated system design, this approach is not supported. The development of the system is introduced from a different perspective, with a focus on the "piezoelectric energy harvesting" system that was previously discussed in **Question 9.** The majority of mechanical engineers engage in research on mechanical systems, procuring piezo-bimorph components and equipment for measuring current and voltage. In contrast, electrical engineers concentrate on the harvesting electric circuit, utilizing commercially available piezoelectric components. The role of materials engineers encompasses the development of piezoelectric compositions and the optimization of structural designs, particularly in the context of unimorph and bimorph configurations. The reader is requested for engaging with the development predicaments intrinsic to these disparate strategies.

Solution: Since the advent of the 21st century, the subject has garnered considerable scholarly attention, particularly with respect to its sustainability and renewable energy characteristics. The advent of piezoelectric damping technology for the purpose of mitigating engine noise and vibration can be traced back to the 1980s [23]. However, following the 1990s, the cyclic electric field excited in a piezoelectric plate by environmental noise vibration is accumulated into a rechargeable battery without being consumed as Joule heat. The Penn State research group has developed energy-harvesting piezoelectric devices based on a "cymbal" structure (29 mm ϕ, 1–2 mm thick). These devices have the capacity to generate electric energy up to 100mW under an automobile engine vibration at 100 Hz [27, 28]. The development of a washer-like energy-harvesting sheet for a hybrid-car application, which combines three cymbals in a rubber composite, has been achieved. This innovation aims to achieve a 1-W-level constant accumulation to a fuel cell. Following the development of our pioneering practical products, it is gratifying to observe a substantial increase in research publications in this field. Nonetheless, I must concede that I felt a sense of embarrassment upon encountering such a multitude of absurd publications as on:

- Energy harvesting from an elastically-hard steel structure with an elastically soft piezo-material — This is a problem from mechanical impedance mismatch
- Unrealistic energy harvesting from a high-frequency (100 kHz) resonant state — Natural noise does not have such a high frequency. Wind, water current = 0.1 – 0.5 Hz; bridge, building, human motion = 1 – 5 Hz; motor, engine = 50 – 100 Hz
- Very small energy harvesting (μW) from MEMS structures — The reported value is lower than that the harvesting circuit consumes (~milliwatts). We usually see microwatts used in sensors, not in energy harvesting.

As previously delineated in Section 2.9, in the energy harvesting system, three successive domains are identified: (i) "mechanical-mechanical energy transfer," which encompasses the mechanical stability of the piezoelectric transducer under substantial stresses and mechanical impedance matching; (ii) "mechanical-electrical energy transduction," relating to the electromechanical coupling factor in the composite transducer structure; and (iii) "electrical-electrical energy transfer," which includes electrical impedance matching, such as a DC/DC converter to accumulate energy into a rechargeable battery. It is important to note that these three domains are interconnected; that is to say, the optimized solution obtained in each distinct domain provides only the "local minimum," not the "overall minimum" solution.

Despite the considerable investments and research endeavors currently directed towards MEMS/NEMS and 'nano harvesting,' there remains a paucity of evidence supporting the efficacy of these approaches. The author's evaluation of the present research endeavors is regrettably not favorable. While medical applications may be considered a desirable aspiration, the energy levels obtained or reported range from picowatts to nanowatts. This range is considered inadequate due to the inherently 'limited volume' of piezoelectric material utilized, typically in the form of thin films. It is imperative to note that medical devices such as micro liquid flow in the body and pacemaker driver necessitate a minimum of 10 mW and 0.5 mW, respectively. In order to reach the targeted output energy of 1 mW, two approaches are considered: (1) the use of a thick piezoelectric film with a thickness greater than 30 μm, even if the area is 3×3 mm^2, and (2) the synchronous accumulation of 1,000 devices. The author, therefore, strongly encourages present researchers to discover a genius idea on how to combine thousands of these nano-devices in parallel and synchronously in phase, in order to reach the obtainable energy level of up to milliwatts.

Reminder: The development of sophisticated device systems encompasses numerous domains, including (i) the transfer of mechanical input into the "transducer," (ii) the transduction of mechanical energy into electrical energy within the transducer, and (iii) the accumulation of electrical output from the transducer. It is imperative to acknowledge the interconnected nature of these three domains. This finding indicates that the optimized solution obtained in each distinct domain offers a "local optimum" but not the optimal solution on a global scale.

BEST-SELLING DEVICES

Question 12: In order to enhance the performance of a system, recent researchers have been integrating supplementary components into the original design. To illustrate, in order to upgrade the positioning resolution to 10 nm on the linear stage, with the original resolution being 1μm, an additional motor is integrated, thereby rendering the control system considerably more complex. This approach is referred to as "Spaghetti Syndrome," and it is not widely endorsed. The predominant opinion among researchers is that enhancing the performance of the device is the optimal strategy for achieving success in

the "best-selling" category. This assertion is not supported by the evidence from the perspectives of industry or manufacturing. In collaboration with Samsung Electromechanics, Korea, the ICAT/Penn State developed a zoom/focus camera module for mobile phones with two micro rotary motors (Figure 23(c)) in the early 2000s. A sophisticated motor, the world's smallest at the time, was constructed using a PZT tube motor. This motor is illustrated in Figure 23(a). The motor was adopted on the cover page of the IEEE Transaction. The "PZT tube type" is characterized by a PZT hollow cylinder with a radial poling direction. The four segmented electrodes on the cylinder surface were exposed to a four-phase (sine, cosine, - sine, - cosine) voltage, thereby inducing a "wobbling" vibration on the tube, akin to a Hula-Hoop motion, to actuate a rotor. While the motor's performance metrics, including rotation speed, torque, power, and size, met expectations, the Samsung VP did not adopt this design for its camera module component. A discussion of the reasons from the perspective of commercialization strategy is requested. Subsequently, the merits of the "metal tube motor" of the final design illustrated in Figure 23(b) should be examined.

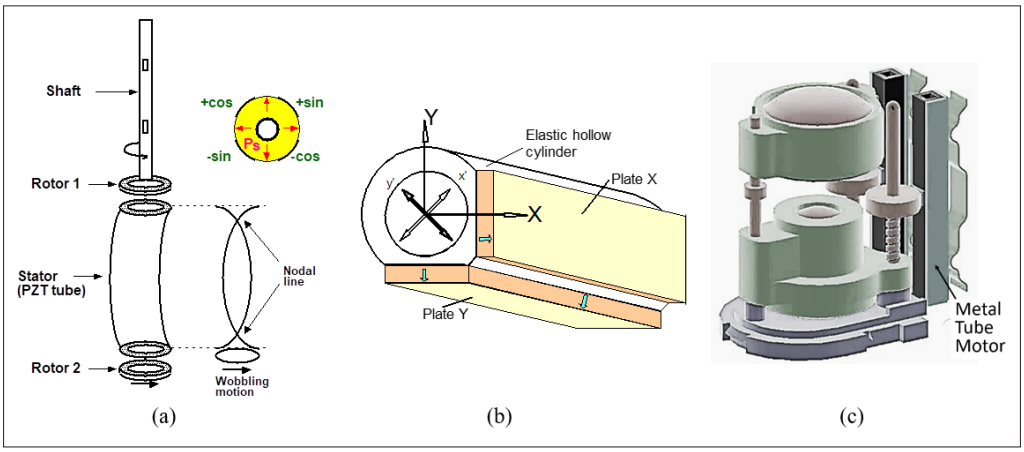

Figure 23: (a) Structure and vibration mode of the PZT tube motor [34], (b) structure of the metal tube motor [35], and (c) camera module with two ultrasonic motors by Samsung Electromechanics

Solution: In the mid-1980s, Akio Morita, the then-president of Sony Corporation of Japan, responded to criticism from a U.S. journalist concerning the apparent lack of "creativity" among Japanese researchers. In response to the criticism, Morita stated, "Japanese researchers are adept at pursuing and imitating the original idea for commercialization, but they generally lack creativity." Morita (2023) posited a tripartite model of creativity in relation to research and development at Sony. The author asserts that the American populace is predominantly oriented towards a narrow interpretation of creativity, namely "technological creativity." However, it is imperative for the public to acknowledge the existence of two additional facets of creativity: "product planning creativity" and "marketing creativity." These aspects are equally crucial for achieving commercial success.

The rejection of the 'PZT tube motor' for the Samsung new camera module application came mainly from the following two problems:

(1) **Cost:** PZT rectangular plate (2 ¢) → disk (5 ¢) → ring (10 ¢) → cylinder (40 ¢). Since Samsung was seeking the price target ~ 40 ¢, including the motor and driver, 40 ¢ just for a PZT tube does not match.

(2) **Durability:** In the context of mobile phone applications, a durability test is imperative. This test involves subjecting the application to 5G shocks from a height of 2 meters, repeatedly, for a total of 1,000 cycles. It is imperative to consider the frequency with which readers drop their mobile phones on a daily basis. The PZT tube failed to withstand the shock test.

Consequently, our Penn State team developed the 'metal-tube type,' which consists of a metal cylinder and two PZT rectangular plates, by slightly sacrificing motor performance due to the reduced PZT volume [See Figure 23(b)] [35]. In the event of driving one of the PZT plates (hereafter referred to as "Plate X"), a bending vibration is excited along the x axis. However, due to an asymmetrical mass (see "Plate Y"), an additional hybridized bending mode is excited. The y axis exhibits a phase lag, resulting in an elliptical locus that rotates in a clockwise direction. This phenomenon bears a resemblance to the motion of a Hula-Hoop when rotated around a PZT-tube type. [35, 36] The rotor of this motor is a cylindrical rod with a pair of stainless ferrule pressed with a spring. The camera module application demonstrated an adequate performance level, with a no-load speed of 1800 rpm and an output torque of 1.8 mN·m under an applied voltage of 80 V_{rms}. This performance level corresponds to a maximum efficiency of approximately 28%. It can be posited that the "second-rank" design was selected from the perspective of "technological creativity."

The author introduces a fundamental "product planning strategy" and procedure for narrowing the development focus below.

Listing All the Possible Application Fields

When we invented piezoelectric actuators, we considered initially various application fields:

1. Office equipment (Printer, Fax machine)
2. Cameras
3. Automobiles

It is imperative to ascertain the sequence of priority in the development of these application areas. The author will introduce the so-called strategic or "managerial decision-making" procedure in the simplest way, using this practical example

Starting with the Simplest Specifications

In the pursuit of identifying a suitable technological specification, a concerted effort was made to identify the most elementary solution. Initially, the restrictions promulgated by the International Organization of Standard (ISO) were given due consideration.

Temperature range – The standard temperature requirements for office equipment range from 20 to 120 ℃. In the case of cameras, despite their frequent use in outdoor settings, they are typically held in the user's hand. Consequently, the temperature is meticulously regulated within the range of 0 to 40°C. At temperatures significantly higher than this, the film will sustain damage before the camera itself is destroyed. The specifications for contemporary digital cameras have undergone modifications, with the lithium-ion battery usage now constituting a novel restriction. Conversely, requirements for automobile applications encompass a significantly broader spectrum: The range of temperatures is from -50 °C to 150 °C.

Durability – The standard requirement for the lifetime of office equipment, such as printers, is defined as continuous operation for a minimum period of three months or 10^{11} cycles, as determined by the manufacturer. For film cameras, the number of cycles is 5×10^4. It is estimated that the average person takes approximately one million pictures in a year. A 36-exposure roll of film can require several months to be utilized. The implementation of the digital camera application necessitates a duration that is hundreds of times the amount of time required for its use. Automobile applications generally necessitate durability that exceeds 10 years. Additional specifications may encompass a range of evaluations, including mechanical shock/drop, humidity, and air pressure (applications in the domains of aerospace and space exploration).

In conclusion, the sequence for starting development will be: Camera > Office Equipment > Automobile.

As anticipated, the initial widespread commercialization of piezo-actuators occurred in the automatic focusing mechanism of Canon film cameras and the shutter mechanism of Minolta cameras. Subsequently, they were employed in dot-matrix (NEC) and inkjet (Seiko EPSON) printers. Since piezo-multilayer actuators have been utilized in diesel injection valves (automobiles) by Siemens in the 2000s, it can be posited that "the piezoelectric actuator development is in a maturing period." A significant shift in camera specifications occurred with the transition from film to digital formats. Digital cameras diverge from traditional film cameras and mechanical shutter cameras due to their unique operational characteristics. This divergence results in specifications that are considerably more stringent. It has been determined that the standard durability is not 5×10^4 cycles anymore. The number of cycles has increased significantly, as users have increasingly opted for higher storage capacities, leading to a substantial increase in the number of pictures or movies captured. The cyclic lifetime specifications have been observed to automatically increase by a factor of 100 in the case of digital cameras.

Considering the Cost Performance

The utilization of a "scoring table" is periodically employed to facilitate the identification of a developmental objective. The process of identifying the most suitable development devices is illustrated in Figure 24 [37]. This table incorporates a range of factors deemed essential, encompassing financial aspects such as market dynamics and cost considerations, along with device performance metrics. A comparison of the total scores is then conducted to determine the projects to prioritize for development, thereby establishing a "pecking order." The motor performance of the PZT-tube is superior to that of the Metal-tube, while the Metal-tube demonstrates resilience in the shock test. As was initially asserted, the metal-tube type is considerably more economical in terms of raw materials and manufacturing cost, a consequence of the most economical rectangular plate PZT usage. With regard to the marketing strategy, clients have expressed a lack of understanding regarding the internal workings of the device, specifically the distinction between the PZT-tube and the Metal-tube. It has been noted that this confusion does not stem from a lack of awareness regarding the importance of the device's specifications.

	Device A PZT tube	Device B Metal tube
High Performance		
1) figure of merit	0 1 (2)	0 (1) 2
2) Lifetime (shock test)	0 (1) 2	0 1 (2)
Cheap Cost		
3) raw materials cost	(0) 1 2	0 1 (2)
4) preparation cost (machining, electroding)	(0) 1 2	0 1 (2)
5) labor cost (special skill)	0 (1) 2	(0) 1 2
Good Market		
6) design	0 1 (2)	0 1 (2)
7) production quantity	0 1 (2)	0 1 (2)
8) maintenance service	0 1 (2)	0 1 (2)
Total score	10	13

Figure 24: Scoring table for PZT-tube and Metal-tube motors for mobile phone applications

Matketing Strategy

As illustrated in Figures. 25(a) and (b), the model represents the inaugural camera module for Samsung flip cell phones, which entered the commercial market in 2003. Newscale Technologies (Victor, NY) integrated a screw in the metal tube motor and commercialized "squiggle motors" worldwide for camera module applications through partnerships with ALPS, Tamron, and TDK-EPC [38]. The utilization of PZT multilayer plates, which replace the conventional rectangular plates, facilitates the operation of squiggle motors at an input voltage of less than 3 V. This characteristic renders them well-suited for integration into compact, portable equipment with ease. Samsung Electromechanics has recently adopted the use of significantly smaller micro ML chip linear USMs for the camera modules of the Galaxy series, a development primarily driven by the need for a thinner design [39]. Refer to Figures 25(c) and (d) for a visual representation of the current camera module utilized in Samsung Galaxy 6S smartphones in 2016. Over the course of 13 years, the physical dimensions of the camera module underwent a substantial reduction, decreasing by a factor of 1/20.

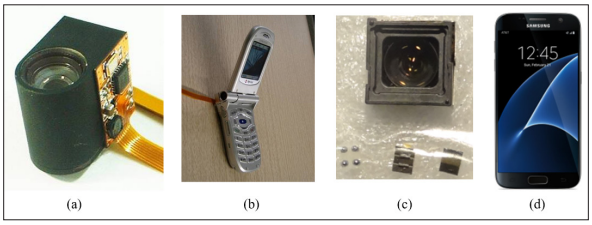

Figure 25: (a), (b) World first camera module for Samsung flip cell phones (2003), and (c), (d) current camera module for Samsung Galaxy 6S smart phones (2016)

Reminder: There are three "creativities" during the "product development." (i) "Technological Creativity" – The sequence for initiating development, otherwise known as the "development pecking order," should be determined based on a company's technological capabilities and the extent of its technological expertise. (ii) "Product Planning Creativity" – Subsequently, a "Scoring Table" can be utilized to narrow down the development focus by considering multiple product designs in terms of "performance," "cost," "reliability," and "market." Selecting the best suitable product with the highest score, a suitable manufacturing method should be employed for production. (iii) "Marketing Creativity" – The creation of distinct customer layers is imperative for the final selection of product design, which is contingent upon the targeted customer base.

CONCLUDING REMARKS

The individual responsible for my supervision during the completion of my doctoral studies was Late Professor Shoichiro Nomura, who was employed at the Tokyo Institute of Technology (presently known as the Institute of Science Tokyo). Upon joining the laboratory, the researcher was instructed to prioritize hands-on learning over the conventional practice of reading papers. The fundamental question is what the true meaning of this phenomenon is. During my undergraduate studies, I obtained what were considered to be "high academic grades." A comprehensive review of relevant literature has been conducted through the analysis of numerous textbooks and academic journals. Consequently, whenever Professor Nomura proposed that I undertake a new research topic, I would respond with remarks such as, "That research has already been conducted by Dr. XYZ, and the results were not promising..." Subsequent to partaking in numerous such exchanges characterized by a negative sentiment, which manifested as a combination of anger and disappointment, Professor Nomura issued the following directive: "Hey, Kenji! For a period of six months, the reading of academic papers is strictly prohibited. It is imperative to approach the subsequent experiment with a neutral stance, devoid of any preconceived notions or biases." A strong bias has been shown to impede the capacity for novel discoveries. Subsequent to the termination of the experiment and the summary of results, the researcher is permitted to consult extant published papers to ascertain the rationality of the observed results and to determine whether they can be explained by existing theoretical frameworks. Initially, I experienced significant trepidation regarding the possibility of obtaining erroneous results. Notwithstanding these challenges, the task was successfully completed. This preliminary observation gave rise to the following hypothesis: The focal point of this inquiry pertains to PMN-PT electrostrictive materials.

The present of the author situation is analogous to a dilemma previously encountered by the late Professor Nomura with regard to his research associates. They consistently seek to utilize Google Search or other AI searching tools to locate research papers. The researchers initiate their research with this biased knowledge in order to align the experimental results with previous studies. It is imperative to acknowledge that an abundance of knowledge can potentially hinder the emergence of novel concepts and initiatives. It is a commonly held belief that significant discoveries are frequently made by engineers who are in the early stages of their careers and therefore have less experience. It is unfortunate, but a certain degree of creativity is often lost upon attaining the status of expert professor. It appears that the "creativity" is deteriorating in tandem with the augmentation of "knowledge," with the exception of fundamental concepts. It is evident that the utilization of AI software such as Google Chat, ChatGPT, and Copilot, prior to the culmination of the research process, has a deleterious effect on the inventive creativity of the researcher.

The author's objective is to facilitate the reader's acquisition of a comprehensive understanding of piezoelectric actuators, thereby empowering them to engage in informed discussions with superiors, peers, and colleagues regarding the development with a heightened level of confidence. It is imperative that the pursuit of breakthroughs and innovations in piezoelectric devices be undertaken with a solid foundation of fundamental knowledge, rather than merely pursuing the developments of other researchers through the use of AI-assisted software. It would be unadvisable to accept the following justification from my associates: The researcher elucidated the rationale behind the action in question, attributing it to the precedent set by a preceding researcher.

ACKNOWLEDGEMENTS

The author acknowledges the contributions of their former associates, who, through their engagement with journal articles, have accumulated a series of misconceptions. The realization of this article would not have been possible without the contributions of these individuals. Additionally, the research fund support from the US Office of Naval Research to ICAT/ Penn State University (N00014-17-1-2088, N00014-20-1-2309) is also acknowledged.

REFERENCES

1. Uchino K. Ferroelectric devices & piezoelectric actuators. 2017.
2. Uchino K. Ferroelectric devices 2nd edition. 2010.
3. Uchino K. Micromechatronics 2nd edition. 2019.
4. Uchino K. Introduction to piezoelectric actuators: research misconceptions and rectifications. Jpn J Appl Phys. 2019. 58: SG0803.
5. Uchino K. Introduction to piezoelectric actuators: research misconceptions and rectifications - part II. Insight - material science. 2019. 2: 1.
6. Uchino K, Yoshizaki M, Kasai K, Yamamura H, Sakai N, et al. New monolithic actuator "monomorph" utilizing semiconductive ferroelectrics. J Jpn Ceram Soc. 1987. 7: 60-63.
7. Uchino K, Yoshizaki M, Kasai K, Yamamura H, Sakai N, et al. Monomorph actuators using semiconductive ferroelectrics. Jpn J Appl Phys. 1987. 26: 1046-1049.

8. Uchino K, Yoshizaki M, Kasai K, Yamamura H. Monomorph characteristics in lead zirconate-based ceramics. Jpn J Appl Phys. 1987. 26: 1252-1255.
9. Uchino K, Yoshizaki M, Nagao A. Monomorph characteristics of Pb (Zr,Ti)O3 based ceramics. Ferroelectrics. 1989. 95: 161-164.
10. Uchino K. High-power piezoelectrics and loss mechanisms. 2020.
11. Gao Y, Uchino K, Viehland D. Effects of thermal and electrical history on "hard" piezoelectrics: a comparison of internal dipolar fields and external DC bias. J Appl Phys. 2007. 101: 054109.
12. Muralt P. Piezoelectric thin films for MEMS. Integrated ferroelectrics. 1997. 17: 297-307.
13. Chen HD, Udayakumar KR, Gaskey CJ, Cross LE, Bernstein JJ, et al. Fabrication and electrical properties of lead zirconate titanate thick films. J Am Ceram Soc. 1996. 79: 2189-2192.
14. Pérez de la Cruz J, Joanni E, Vilarinho PM, Kholkin AL. Thickness effect on the dielectric, ferroelectric, and piezoelectric properties of ferroelectric lead zirconate titanate thin films. J Appl Phys. 2010. 108: 114106.
15. Gao P, Zhang Z, Li M, Ishikawa R, Feng B, et al. Possible absence of critical thickness and size effect in ultrathin perovskite ferroelectric films. Nature communications. 2017. 15549.
16. Du XH, Belegundu U, Uchino K. Crystal orientation dependence of piezoelectric properties in lead zirconate titanate: theoretical expectation for thin films. Jpn J Appl Phys. 1997. 36: 5580-5587.
17. Wasa K. Proc 69th ICAT int'l smart actuator symp. 2016.
18. Uchino K, Sadanaga E, Oonishi K, Yamamura H. Ceramic dielectrics. 1990. 8: 107.
19. Yano K, Inoue T, Takahashi S, Fukui I. Proc EE annual meeting. 1984.
20. Fujii A. Proc smart actuators/sensors study committee. 2005.
21. Sugiyama S, Uchino K. Pulse driving method of piezoelectric actuators. Proc IEEE int'l symp appl of ferroelectrics. 1986.
22. Uchino K. Piezoelectric actuators and ultrasonic motors. 1997.
23. Uchino K, Ishii T. Mechanical damper using piezoelectric ceramics. J Jpn Ceram Soc. 1988. 96: 863-867.
24. Uchino K. Essentials of piezoelectric energy harvesting. 2021.
25. Muensit N. Energy harvesting with piezoelectric and pyroelectric materials. 2011. 72.
26. Uchino K, Ishii T. Energy flow analysis in piezoelectric energy harvesting systems. Ferroelectrics. 2010. 400: 305-320.
27. Kim HW, Priya S, Uchino K, Newnham RE. Piezoelectric energy harvesting under high pre-stressed cyclic vibrations. J Electroceramics. 2005. 15: 27-34.
28. Kim HW, Priya S, Uchino K. Modeling of piezoelectric energy harvesting using cymbal transducers. Jpn J Appl Phys. 2006. 45: 5836-5840.
29. Shekhani H, Scholehwar T, Hennig E, Uchino K. Characterization of piezoelectric ceramics using the burst/transient method with resonance and antiresonance analysis. J Am Ceram Soc. 2017. 100: 998.
30. Ural SO, Tuncdemir S, Zhuang Y, Uchino K. Development of a high-power piezoelectric characterization system (HiPoCS) and its application for resonance/antiresonance mode characterization. Jpn J Appl Phys. 2009. 48: 056509.
31. Zhuang Y, Ural SO, Tuncdemir S, Amin A, Uchino K. Analysis on loss anisotropy of piezoelectrics with ∞mm crystal symmetry. Jpn J Appl Phys. 2010. 49: 021503.
32. Uchino K, Zhuang Y, Ural SO. Loss determination methodology for a piezoelectric ceramic: new phenomenological theory and experimental proposals. J Adv Dielectrics. 2011. 1: 17-31.
33. Shekhani HN, Uchino K. Evaluation of the mechanical quality factor under high power conditions in piezoelectric ceramics from electrical power. J Eur Ceram Soc. 2014. 35: 541-544.
34. Dong S, Lim SP, Lee KH, Zhang J, Lim LC, et al. Piezoelectric ultrasonic micromotors with 1.5 mm diameter. IEEE UFFC Trans. 2003. 50: 361-367.
35. Koc B, Cagatay S, Uchino K. A piezoelectric motor using two orthogonal bending modes of a hollow cylinder. IEEE UFFC Trans. 2002. 49: 495-500.
36. Cagatay S, Koc B, Uchino K. A 1.6 mm metal tube ultrasonic motor. IEEE UFFC Trans. 2003. 50: 782-786.
37. Uchino K. Entrepreneurship for engineers. 2009.
38. New scale technologies. 2026.
39. Koc B, Ryu J, Lee D, Kang B, Kang BH, et al. Proc new actuator. 2006.